



Published in final edited form as:

*Arterioscler Thromb Vasc Biol.* 2019 March ; 39(3): 413–431. doi:10.1161/ATVBAHA.118.312191.

## POTENTIAL ROLE OF H-FERRITIN IN MITIGATING VALVULAR MINERALIZATION

Katalin Éva Sikura<sup>1,2,+</sup>, László Potor<sup>1,2,+</sup>, Tamás Szerafin<sup>2,3</sup>, Abolfazl Zarjou<sup>4</sup>, Anupam Agarwal<sup>4</sup>, Paolo Arosio<sup>7</sup>, Maura Poli<sup>7</sup>, Zoltán Hendrik<sup>5</sup>, Gábor Méhes<sup>5</sup>, Melinda Oros<sup>1,2</sup>, Niké Posta<sup>1,2</sup>, Livia Beke<sup>2,5</sup>, Ibolya Fürtös<sup>2</sup>, György Balla<sup>1,6</sup>, and József Balla<sup>1,2</sup>

<sup>1</sup>HAS-UD Vascular Biology and Myocardial Pathophysiology Research Group, Hungarian, Academy of Sciences, Debrecen, Hungary

<sup>2</sup>Department of Medicine, Faculty of Medicine, University of Debrecen, 4012 Debrecen, Hungary

<sup>3</sup>Department of Cardiac Surgery, Faculty of Medicine, University of Debrecen, 4012 Debrecen, Hungary

<sup>4</sup>Department of Medicine, Division of Nephrology, Nephrology Research and Training Center and Center for Free Radical Biology, University of Alabama at Birmingham, Birmingham, AL 35294, USA

<sup>5</sup>Department of Pathology, University of Debrecen, Faculty of Medicine, 4012 Debrecen, Hungary

<sup>6</sup>Department of Pediatrics, Faculty of Medicine, University of Debrecen, 4012 Debrecen, Hungary

<sup>7</sup>Department of Molecular and Translational Medicine, University of Brescia, Brescia, Italy.

### Abstract

**Objective:** Calcific aortic valve disease (CAVD) is a prominent finding in elderly and patients with chronic kidney disease. We investigated the potential role of iron metabolism in the pathogenesis of CAVD.

**Approach and Results:** Cultured valvular interstitial cells (VIC) of stenotic aortic valve with calcification from patients undergoing valve replacement exhibited significant susceptibility to mineralization/osteoblastic transdifferentiation in response to phosphate. This process was abrogated by iron via induction of H-ferritin as reflected by lowering ALP and osteocalcin secretion, and preventing extracellular calcium deposition.

Cellular phosphate uptake and accumulation of lysosomal phosphate were decreased. Accordingly, expression of phosphate transporters Pit1 and Pit2 were repressed. Translocation of ferritin into lysosomes occurred with high phosphate binding capacity. Importantly, ferritin reduced nuclear accumulation of RUNX2, and as a reciprocal effect it enhanced nuclear localization of transcription factor Sox9. Pyrophosphate generation was also increased via up-regulation of

---

Corresponding author: József Balla, M.D., D.Sc., Pf. 19., Nagyerdei krt. 98., 4012 Debrecen, Hungary, Phone/Fax: (36)-30-3371155, balla@belklinika.com.

<sup>+</sup>The authors share the first authorship.

Disclosures

All the authors declared no competing interests.

ENPP2. 3H-1, 2-dithiole-3-thione (D3T) mimicked these beneficial effects in VIC via induction of H-ferritin. Ferroxidase activity of H-ferritin was essential for this function, as ceruloplasmin exhibited similar inhibitory functions. Histological analysis of stenotic aortic valve revealed high expression of H-ferritin without iron accumulation and its relative dominance over ALP in non-calcified regions. Increased expression of H-ferritin accompanied by elevation of TNF- $\alpha$  and IL1- $\beta$  levels, inducers of H-ferritin, corroborates the essential role of ferritin/ferroxidase via attenuating inflammation in CAVD.

**Conclusions:** Our results indicate that H-ferritin is a stratagem in mitigating valvular mineralization/osteoblastic differentiation. Utilization of D3T to induce ferritin expression may prove a novel therapeutic potential in valvular mineralization.

### Keywords

valvular stenosis; arteriosclerosis; chronic kidney disease; phosphate; vascular calcification

---

### Introduction

Calcification and stenotic disease of the aortic valve is a common pathology in the elderly and patients undergoing dialysis characterized by progressive mineralization with significant clinical implications. The exceptional endurance of this thin tissue is made by two types of cells: valvular endothelial cells (VEC) and valvular interstitial cells (VIC) that permanently repair and remodel the tissue of the valve in response to local mechanical and biological signals that potentially involve any of the cardiac valves (Reviewed in [1]). There is substantial histopathologic and clinical data which suggest that calcific aortic valve disease (CAVD) is an active disease process while are differences within the affected tissue. Mostly, the affected valves have heterogeneous areas with calcification and inflammation. Inflammation is a critical initiation step involved in valvular disease as shown by the National Heart Lung and Blood Institute (NHLBI; 2011) and other research groups [1–6].

These observations and the ratio of the calcified and non-calcified regions could guide in distinguishing the state of calcification [2, 7–9]. The clinical significance of vascular and valvular mineralization are highlighted in patients with kidney disease. Calcification of the vascular tree at the level of tunica media and acceleration of aortic valve calcification are cardinal findings in patients advanced chronic kidney disease (CKD) and those undergoing renal replacement therapy [10]. In stenotic aortic valve calcification, VIC can transdifferentiate into myofibroblast-like cells, which are identified by markers of contractility such as alpha smooth muscle actin ( $\alpha$ -SMA), or into osteoblast-like cells, identified by upregulation of ALP activity, and increased levels of osteocalcin expression in later stages.

Rajamannan and colleagues revealed that a marked increase in the expression of Runt-related transcription factor 2 (RUNX2) and SRY (sex determining region Y)-box 9 (Sox9) occurs in aortic valve calcification, which are critical transcription factors in osteoblast differentiation [11, 12]. Subsequently, Lincoln and colleagues identified the unique role for Sox9 in expansion of heart valve progenitors during development [13] and described an inhibitory function of Sox9 on RUNX2-dependent in VIC [14, 15]. These effects are

potentially mediated via the regulation of RUNX2 turnover [16] as well as inhibition of RUNX2 expression in VIC [15].

One of the most potent recognized inducers of vascular calcification is elevated plasma phosphate level in CKD patient [17–19]. It provokes calcification of vascular cells in a process mediated by a sodium-dependent phosphate co-transporter that facilitates entry of phosphate into the cells. Phosphate uptake occurs via phosphate carriers Pit1 and Pit2 [20, 21]. This induces osteoblastic transition of vascular smooth muscle cells via a process that is accompanied by translocation of the RUNX2 from the cytosol into the nucleus that is essential for osteoblast differentiation, bone matrix gene expression, and, consequently, bone mineralization [17–19].

Pyrophosphate (PPi) is a key regulator of tissue calcification via inhibition of mineralization by binding to nascent hydroxyapatite crystals. Ectonucleotide pyrophosphatase/phosphodiesterase-2 (ENPP2) is a cell membrane glycoprotein that generates PPi via cleaving ATP [22]. The ankyrin G1 (ANK1) is a transmembrane protein which has a critical role in the regulation of pyrophosphate metabolism. The main function of ANK1 is transporting intracellular PPi into the extracellular space [23].

We previously found that ferritin-ferroxidase activity plays an important role in downregulation of calcification of vascular smooth muscle cells and the underlying gene expression [24]. Expression of H-ferritin is strongly regulated at a translational level by iron [25, 26] and transcriptional levels by D3T [27, 28] as well as inflammatory cytokines [29, 30]. The objective of this study, therefore, was to investigate how ferritin and its ferroxidase activity may inhibit the mineralization process, or suppress the phenotype transition of VIC into osteoblast-like cells. Furthermore, we examined the similarities and differences between the calcification potential of valvular interstitial cells derived from stenotic aortic valve with calcification (CAVD) labeled AS in the text and isolated aortic valve with insufficiency (AI).

## Materials and Methods

### Disclosure statement

The authors declare that all supporting data are available within the article [and its online supplementary files].

### Cell isolation and culture

Human aortic valve leaflets were obtained between May 2012 to Jan 2017 (161 patients) (Regional Research Ethical Committee, Project No.: 3853–2013 and 4699–2016) from surgical specimens from patients undergoing complete valve replacement for stenosis with calcification (referred to as aortic valve with stenosis (AS) for this study). Aortic valves were received from surgical specimens from patients who had severe insufficiency without calcification (36 valves, referred to them as isolated insufficient aortic valve (AI). Cells were isolated from human heart valves by collagenase (600 U/mL) (EMD Millipore Corp.; 234155–100MG) and cultured as previously described [31].

### Healthy heart valves

Healthy aortic valves for controls were obtained from cadavers (N=13) of suicide or traumatic events without cardiovascular diseases from Department of Forensic Medicine, University of Debrecen (Regional Research Ethical Committee, Project No.: 5038–2018).

### Control VIC primary cells

VIC cells were purchased from Innoprot Ltd. (Parque Tecnológico de Bizkaia, Batch #0960; Spain). The cells were derived from a healthy 8 years old Caucasian male.

### Induction of calcification

At about 80 percent of confluence, VIC was cultured in calcification medium, which was prepared by adding 2.5 mmol/L inorganic phosphate and 1.8 mmol/L calcium-chloride to the growth medium. Both growth medium and calcification medium were changed every second day. For time course experiments, the first day of culture in calcification medium was the defined as day 0.

### Immunofluorescence staining

Mouse monoclonal anti-human  $\alpha$ -SMA (Santa Cruz; sc-3225; 400 ng/mL); rabbit polyclonal anti-human von Willebrand factor antibody (Abcam; ab6994; 100 ng/mL) were used as primary antibodies to identify VIC and endothelium. Then, samples were incubated with secondary antibodies CY3-conjugated Streptavidin (Jackson ImmunoResearch; 016-160-084; 1000 ng/mL); Biotin (Jackson ImmunoResearch; 715-065-150; 1000 ng/mL); respectively. For nuclear translocation of RUNX2, we used rabbit polyclonal anti-human RUNX2 (Proteintech; 20700-1-AP; 60 ng/mL) and labeled with anti-rabbit Alexa Fluor 488 (Thermo Fisher Scientific; A11070; 2000 ng/mL). For LAMP1 and H-ferritin double staining anti-human rabbit anti-human LAMP1 (Abcam; ab24170; 1000 ng/mL) and mouse anti-human H-ferritin (Santa Cruz; sc-376594; 400 ng/mL) were used with secondary antibodies anti-rabbit Alexa Fluor 488 against LAMP-1 (Thermo Fisher Scientific; A11070; 2000 ng/mL); anti-mouse Alexa 647 (Thermo Fisher Scientific; A21244; 4000 ng/mL) against H-ferritin respectively. Sox9 staining was performed with rabbit anti-human Sox9 (Abcam; ab26414; 2000 ng/mL) antibody followed by the anti-rabbit Alexa Fluor 488 (Thermo Fisher Scientific; A11070; 2000 ng/mL) secondary antibody. Hoechst (0.5 ng/mL) was used to stain nuclei. Multicolor STED imaging was acquired with STED (Stimulated Emission Depletion) Leica TCS SP8 gated STED-CW nanoscopy (Leica Microsystem Mannheim, Germany). Gated STED images were deconvolved using Huygens Professional (Scientific Volume Imaging B.V., Hilversum, Netherlands) software.

### Flow Cytometry

Cells were fixed and stained with FITC conjugated mouse anti-human CD31 antibody (Abcam; ab27333) and run on a FACSscan flow cytometer. Cell population was identified and gated based on size (forward scatter, FSC) and complexity (side scatter, SSC). Isotype sample was used as control.

### **Viability assay**

The NUCLEAR-ID® Blue/Red cell viability assay (Enzo Life Sciences; ENZ-53005-C100) was employed by manufacturer's guide. The staining pattern was determined by fluorescence/confocal microscopy (Leica DM2500, and Leica DFC480 digital camera).

### **Nodule quantification and calcium quantification assay**

Valvular interstitial cells grown on cell culture plates until 90% confluent, they were washed twice with PBS and decalcified using 0.6 mol/L HCl for 1 hour. Calcium content of the supernatants was determined by QuantiChrome Calcium Assay Kit (Gentaur). After decalcification, cells were solubilized with a solution of NaOH 0.1 mol/L and SDS 0.1%. Calcium content of the cells was normalized to protein content and expressed as µg/mg protein. Calcium was determined by QuantiChrome Calcium Assay Kit (BioAssays System; DICA-500) and normalized to protein content. Alizarin Red S (Sigma Aldrich; A5533) staining was employed to visualize the calcium deposition. Plates were fixed with 3 % paraformaldehyde, and stored at 4°C for 10 minutes, and stained with a 2 % solution of Alizarin Red S. All calcific nodules in each well were then manually counted under a microscope.

### **Intracellular phosphate content**

Valvular interstitial cells cultured on 12 well plates and lysate by NP40 and Triton-X100 mixed lysis buffer for 1 hour. QuantChrom quantitative colorimetric phosphate assay (BioAssays System; DIPI-500) was employed to measure cellular phosphate level. Phosphate uptake normalized by the protein content of the cells.

### **Quantification of osteocalcin**

Detection of osteocalcin from the extracellular matrix of the cells grown on six-well plates was performed by analyzing the amount of extracellular osteocalcin deposition. The extracellular matrix was dissolved in 300 µL EDTA (0.5 mol/L, pH 6.9). Osteocalcin content of the EDTA-solubilized extracellular matrix samples was quantified by ELISA method (Bender MedSystem; BMS2020INST) [28].

### **Alkaline phosphatase staining**

To visualize alkaline phosphatase, we stained cells with Naphtanol AS-MX –Fast Violet B (Sigma Aldrich; F1631) solution mix [28].

### **Detection of pyrophosphate**

Valve interstitial cells were cultured in 24 well plates in phenol red-free D-MEM (Sigma; D5648) for five days in normal condition or high phosphate and calcium administration. Inorganic pyrophosphate (PPi) was measured in the extracellular fluid of the VIC using PPLight™ inorganic pyrophosphate assay (Lonza; LT-07–610). The continuous kinetic assay was employed according to the manufacturer's instruction. The luminescence was monitored for 2 hours using Synergy™ MHTX Multi-Mode Microplate Reader from BioTek Instruments (USA) with 0.1 s integrated reading time. The relative luminescence (RLU) was normalized to protein content of the cells.

## Nuclear and cytoplasmic protein extraction

Cells were cultured in growth medium and treated with or without calcification medium supplemented with 20  $\mu\text{mol/L}$  AP72. After treatment, cells were harvested with cell scraper and collected into a centrifuge tube. Pellets were washed twice with PBS followed by addition of ice cold 1x cytoplasmic lysis buffer (20 mmol/L Tris-HCl pH 8.0, 100 mmol/L NaCl, 300 mmol/L sucrose, 3 mmol/L  $\text{MgCl}_2$ , protease inhibitor cocktail) to the pellets. Cell suspensions were incubated on ice for 15 minutes. After centrifugation, the supernatants were collected (contains cytoplasmic proteins), the pellets were washed with PBS and resuspended in ice-cold nuclear extraction buffer (20 mmol/L Tris-HCl pH 8.0, 300 mmol/L NaCl, 2 mmol/L EDTA pH 8.0, protease inhibitor cocktail). Next, the samples were drawn 5 times with 27 gauge needle for the extraction of the nuclear proteins followed by centrifugation at 8000x g, 4°C for 20 minutes. The supernatant contains the nuclear fraction. The protein concentration of the samples was determined by the BCA Protein Detection Kit (Amersham).

## Western Blot analysis

H-ferritin Western blotting was performed with rabbit anti-human H-ferritin antibody (Santa Cruz; sc-376594; 400ng/mL), followed by HRP-labeled anti-rabbit IgG antibody. To detect Pit-1, Pit2 and LAMP1 were used rabbit anti-human Pit1 antibody (Abcam; ab177147; 2000 ng/mL), rabbit anti-human Pit2 antibody (Proteintech; 12820-1-AP; 60 ng/mL), rabbit anti-human-LAMP1 antibody (Abcam; ab24170; 1000 ng/mL). Western blot analysis for ENPP2 was performed using anti-human ENPP2 (Thermo Fisher Scientific; PA5-12478; 4000 ng/mL). Sox9 Western blot was performed with rabbit anti-human Sox9 (Abcam; ab26414; 2000 ng/mL). Western blots were performed with: rabbit anti-human Sox9 (Abcam; ab26414; 2000 ng/mL) and rabbit anti-human RUNX2 (Proteintech; 20700-I-AP; 400 ng/mL); rabbit anti-human TNF- $\alpha$  (Thermo Fisher Scientific; PA5-19810; 400 ng/mL); rabbit anti-human IL1- $\beta$  (Invitrogen; 17h18116; 400 ng/mL). Complexes of antigen-antibody were visualized with a horseradish peroxidase chemiluminescence detection system (Amersham Biosciences; RPN2109). Membranes were reprobred with glyceraldehyde-3-phosphate dehydrogenase (GAPDH).

## Ferritin gene silencing

VIC was cultured in 12 well plates and at about 80 percent of confluence, cells were transfected with siRNA against H-ferritin (Ambion; s225998) for 4 hours in minimal serum-content medium (Opti-MEM; Gibco; 31958-047; Lot.: 1782606). At the end of transfection cells were washed with PBS three times and 30 % FBS containing, antibiotic free D-MEM was added. Next day cells were washed and treated with iron or D3T for two times until five days.

## Isolation of lysosomes

To separate lysosomes, we used the Lysosome Enrichment Kit for Tissue and Cultured Cells (Thermo Fisher Scientific; 89839) and gradient ultracentrifugation. For protein analysis, lysosomes were lysed with 2 % CHAPS (Sigma Aldrich; C2632-25G) in Tris-buffered saline (TBS; 25 mmol/L Tris, 0.15 mol/L NaCl; pH 7.2) samples were centrifuged with

Beckman ultracentrifuge at 38000 x g and the lysosomal fractions were collected from each sample.

### Immunohistochemistry

Heart valve tissues were fixed with formaldehyde for one day followed by TRIS buffer and embedded in paraffin wax. Subsequently, slides were deparaffinized in xylene for 5 minutes and then rehydrated. For immunohistochemistry, slides were subjected to a peroxidase-blocking reagent for 5 minutes (3% hydrogen peroxide was used to block endogenous peroxidase activity). Antigen retrieval was performed in an epitope retrieval solution (Leica RE-7113) at pH 6 using a pressure cooker (rice programs, IDA Avair 6 L pressure cooker). Double immunostaining of ALP-H-ferritin interaction was performed sequentially with the EnVision FLEX/HRP system. Following the first IHC staining terminating with the EnVision FLEX/HRP detection step, the incubation with the second primary monoclonal antibody was performed. In addition to DAB (brown color), the chromogen VIP was used to highlight the second IHC reaction in a different color (dark violet). For double staining experiments, methyl-green counterstaining was performed. Samples were incubated with the following primary antibodies: rabbit anti-human ALP antibody (Abcam; ab65834; 1000 ng/mL); mouse anti-human H-ferritin antibody (Santa Cruz; sc376594; 400 ng/mL). Other IHC stains were performed with the following antibodies: rabbit anti-human TNF- $\alpha$  (Thermo Fisher Scientific; PA5-19810; 400 ng/mL); rabbit anti-human IL1- $\beta$  (Invitrogen; 17h18116; 400 ng/mL). Antibody binding was visualized by the Super Sensitive TM One Step Polymer-HRP IHC Detection System. The intensity and distribution of antibodies expression were assessed by light microscopy (Leica DM2500 microscope, DFC 420 camera and Leica Application Suite V3 software, Wetzlar, Germany). ALP and H-ferritin colocalization of the IHC samples were measured by Image J software.

### Prussian Blue staining

Prussian blue reaction involves the treatment of sections with acid solutions of ferrocyanides. Any ferric ion ( $\text{Fe}^{3+}$ ) present in the tissue combines with the ferrocyanide and results in the formation of a bright blue pigment called Prussian blue, or ferric ferrocyanide. Heart valve tissues were fixed with 10 % neutral buffered formaldehyde for two days followed by decalcination (EDTA-TRIS buffer) and embedded in paraffin wax. 4  $\mu\text{m}$  slides were then deparaffinized for further staining. For special staining, slides were incubated in 5% potassium ferrocyanide and 5% hydrochloric acid containing solution for 30 minutes in fume hood. Nucleus staining was performed in Gallego solution for 5 minutes and samples were dehydrated. The intensity and distribution of ferrocyanide complex were assessed by light microscopy (Leica DM2500 microscope, DFC 420 camera and Leica Application Suite V3 software, Wetzlar, Germany).

### Measurement of colocalization

Measurement of colocalization percent was analyzed by Leica Application Suite (LAS) X software.

## Statistical analysis

Data were analyzed by GraphPad Prism 5.02 software (GraphPad Software Inc., 7825 Fay Avenue, Suite 230 La Jolla, CA 92037). All statistical data are expressed as mean  $\pm$  SEM. If data groups passed normality test and equal variance test, we performed Student's t-test or One Way ANOVA followed by Bonferroni post hoc tests as indicated in figure legends.  $P < 0.05$  was considered significant.

## Results

### Iron, D3T, and apo-ferritin (AF) markedly mitigate VIC calcification process

Based on our previous investigations that identified induction of H-ferritin as an inhibitory mechanism against osteoblastic transition of vascular smooth muscle cells [10] we tested whether elevation of intracellular level of H-ferritin would mimic these effects in VIC. Iron and D3T were utilized to induce the expression of H-ferritin in VIC. Calcification medium alone significantly increased the extracellular calcium content of cultured VIC. Iron and D3T significantly decreased the extracellular calcium in a dose-dependent manner (Figure 1 and Supplementary Figure I. A and B) and the expression of osteocalcin, respectively. Apo-ferritin (devoid of iron) also inhibited the extracellular calcium deposition and osteocalcin level of VIC (Figure 1A middle and right panel). These observations were supported by Alizarin Red S staining after five days (Figure 1B). Next, we asked whether inhibition of the mineralization pathway of VIC also relies on H-ferritin/ferroxidase. Indeed, we show that upregulation of H-ferritin via iron or D3T or supplementation with apo-ferritin prevents calcium deposition as well as expression of osteocalcin. Figure 1C and 1D show the elevated H-ferritin levels after exposure to iron, apo-ferritin or D3T. Supplementary Figure II. C and D show the densitometry of H-ferritin expression. To further confirm the importance of the inhibitory role of H-ferritin, we transfected VIC with small interfering RNA (siRNA) specific to H-ferritin. In the presence of H-ferritin siRNA, iron or D3T failed to inhibit calcification as reflected by the accumulation of calcium and osteocalcin (Figure 1D and E). Supplementary Figure II. A and B confirm silencing of H-ferritin expression in VIC.

To validate the ferroxidase activity's paramount role in inhibition of mineralization, we used another protein that possesses this activity, namely ceruloplasmin. As shown in Supplementary Figure III. A and B mineralization of VIC in calcifying condition was inhibited by ceruloplasmin or H-ferritin as reflected by decreased calcium content of extracellular matrix that was also confirmed by Alizarin Red S staining.

Induction of H-ferritin by iron or D3T in cells derived from healthy subjects, as well as administration of recombinant H-ferritin but not mutant H-ferritin<sup>222</sup> lacking ferroxidase activity, prevented mineralization of VIC as reflected by accumulation calcium and osteocalcin in the extracellular matrix (Supplementary Figure IV. A and B).

### Calcification potential of VIC derived from isolated insufficient aortic valve and stenotic aortic heart valves

Next, we investigated whether the origin of VIC (cells derived from the aortic valve with insufficiency (AI) or stenotic valve leaflets (AS) may influence the calcification potential of

these cells. Supplementary Figure V. shows that cells from stenotic valve tissue have greater ability to transdifferentiate into osteoblast-like cells as indicated by the higher level of extracellular calcium deposition and the accumulation of calcium binding protein, osteocalcin (Supplementary Figure V. A and V. B). Furthermore, we found that the inhibitory effect of iron and apo-ferritin on mineralization was more pronounced in AI valve cells compared to AS VIC. In Supplementary Figure V. we demonstrate that calcium accumulation and osteocalcin levels were higher in AS compared to AI VIC. Interestingly, iron exposure could not inhibit mineralization in the AS stage VIC compared to AI VIC. However, apo-ferritin treatment could inhibit calcification regardless the degree of valvular disease. This is likely explained by the high concentration of apo-ferritin and may suggest that significantly higher levels of iron may exert similar effects. Osteocalcin, the important marker of osteoblastic activity, also corroborated the above findings and its levels suggested that apo-ferritin had a paramount effect on its expression than iron (Supplementary Figure V. B). Macroscopic images from AI and AS valves are shown in the Supplementary Figure V. C.

### **Accumulation of nuclear RUNX2 is inhibited by iron, apo-ferritin and D3T**

Runt-related transcription factor 2 (RUNX2) is a key determinant of osteoblast activity [32] and implicated in the pathogenesis of vascular mineralization [33]. Therefore, we investigated whether regulation of osteoblastic differentiation of VIC by ferritin occurs via modulation of RUNX2. We examined cultured VIC by immunocytochemistry and by Western blot (Figure 2A and 2B) and found nuclear translocation of RUNX2 in cells maintained in calcification medium. On the contrary, treatment of VIC with iron, apo-ferritin, or D3T prevented translocation of RUNX2 into the nucleus (Figure 2A and 2B). Colocalization rate of RUNX2 bound to DNA in the nucleus (Hoechst staining) is shown in Figure 2A. Furthermore, we also tested the location of RUNX2 by immunostaining in VIC derived from AS and its expression from whole protein lysates derived from AS valves as compared to AI valves (Figure 2C and 2D). We found that RUNX2 is located in AS sample's nuclear region. Conversely, nuclear location of RUNX2 was not detected in AI derived VIC (Figure 2D). Moreover, silencing of H-ferritin gene resulted in increased translocation of RUNX2 into the nucleus (Supplementary Figure VI). Lower magnification images of RUNX2 immunostaining with antibody controls are shown in Supplementary Figure VII.

### **Nuclear translocation of Sox9 is enhanced by iron, apo-ferritin and D3T**

Since RUNX2 activity was previously revealed to be antagonized by Sox9 in VIC [16], we investigated the location of Sox9 in cultured VIC by immunocytochemistry and Western blot analysis. In cells cultured in growth medium Sox9 existed in the nucleus, while under calcific conditions nuclear Sox9 was barely detectable (Figure 3A and 3B). In contrast, nuclear location of Sox9 was maintained in cells cultured in calcification medium supplemented with iron, apo-ferritin and D3T. Moreover, we also collected human heart valves of AS exhibiting calcification for comparison to AI without calcification. Western blot analysis showed the nuclear presence of Sox9 in AI valve samples. On the contrary, nuclear Sox9 in AS valves was below the detection level (Figure 3C). Lower magnification images of Sox9 immunostaining with antibody controls are shown in Supplementary Figure VIII.

### **Iron, apo-ferritin, D3T and H-ferritin inhibit the uptake of phosphate in VIC**

Nuclear translocation of RUNX2 was shown to be regulated by intracellular phosphate level [34, 35]. To test whether H-ferritin affects intracellular phosphate levels in VIC maintained in normal condition or calcification medium we treated VIC with iron, apo-ferritin or D3T. As shown in Figure 4A significantly lower intracellular phosphate levels were found in cells exposed to iron, apo-ferritin or D3T compared to cells growing in calcific condition alone. Importantly, lysosomal phosphate level was also decreased to the control level in response to iron exposure in cells cultured in calcification medium (Figure 4B). Accordingly, expression of Pit1 (the membrane-associated channels responsible for the phosphate transport) was attenuated after treatment of VIC with iron, apo-ferritin or D3T (Figure 4C). In addition, Pit2 expression was diminished in response to ferritin induction (Figure 4D). Exogenous H-ferritin also decreased Pit1 protein expression in VIC cells derived from AS tissues (Figure 4E).

### **H-ferritin is associated with inorganic phosphate entry into the lysosome**

Apo-ferritin has a hollow internal cavity which can accommodate iron in a ferric oxyhydrophosphate complex [36]. Through the action of ferroxidase, it is capable of storing iron and phosphate (2250 and 380 atoms, respectively). The amount of iron and phosphate within the core of ferritin are not related to different subunit composition. Double immunostaining against LAMP1 (lysosome marker) and H-ferritin (Figure 5B) revealed maximal co-localization (Figure 5C). Furthermore, inside the fused lysosomes (shown by arrows) a significant accumulation of ferritin is evident. To confirm this finding, we isolated lysosomes from cultured and treated VIC, and tested for H-ferritin/LAMP1 in different conditions: in the growth medium; calcification medium alone, or supplemented with iron. In iron-treated cells, we found a markedly increased H-ferritin level inside the lysosome (Figure 5A) which is demonstrated by the co-localization rate of H-ferritin and LAMP1 (Figure 5C). Lower magnification images of LAMP1- H-ferritin immunostaining with antibody controls were shown in Supplementary Figure IX.

### **Extracellular pyrophosphate plays a critical role in inhibition of valvular calcification**

Pyrophosphate (PPi) is also a key inhibitor of mineralization through binding to nascent hydroxyapatite crystals [37, 38]. Therefore, we analyzed the changes of the level of pyrophosphate compared with the calcification medium. Iron/apo-ferritin/D3T treatment significantly increased the level of pyrophosphate contrary to cultured cells in calcification medium (Figure 6A). Since, ENPP2 is an important pyrophosphate generating ectoenzyme we examined whether ENPP2 expression was correlated with PPi level. Similarly to PPi, a decrease in ENPP2 expression was observed under calcification condition. Intriguingly, elevated expression of ENPP2 and higher PPi level were found in cells exposed to iron, apo-ferritin and D3T as compared to those cultured in calcification medium alone (Figure 6C). Moreover, treatment of cell with H-ferritin also increased ENPP2 protein level in VIC derived from AS tissues (Figure 6E). To confirm the importance of H-ferritin in controlling the pyrophosphate generation, we transfected VIC with small interfering RNA (siRNA) specific to H-ferritin. In the presence of H-ferritin siRNA, iron and also H-ferritin failed to

enhance PPI level (Figure 6B and 6D). Expression of Ankyrin G1 protein was not altered by ferritin (data not shown).

### **High expression of H-ferritin is accompanied with relatively low expression of ALP in non-calcified regions**

The above findings prompted us to examine whether the expression of ferritin is altered in VIC in CAVD. Therefore, Western blot analysis was performed for H-ferritin from patients' tissue lysate samples of AS and AI. Significantly higher level of H-ferritin was present in AS when compared to AI valves (Figure 7A). To localize H-ferritin in CAVD dual immunohistochemistry investigation (ALP and H-ferritin) was carried out. As shown in Figure 7B, ALP<sup>+</sup> and H-ferritin<sup>+</sup> cells were present in the affected valve from the endothelial surface to the calcific core. In the distant surface area more H-ferritin and less ALP staining was observed in cells, the ratio was 2.3:1 ±0.41, respectively. Expression of ALP and H-ferritin progressively increased toward the core and the ratio of H-ferritin to ALP decreased to 0.6 ±0.15 at the zone close to the calcific core of AS. In AI valves the staining for ALP and H-ferritin was even and moderate, the ratio of H-ferritin to ALP was 2.2:1±0.65 (Figure 7B).

### **Increased H-ferritin level in AS valves is accompanied by inflammatory markers without the accumulation of iron**

Our previous findings highlight the question as to whether the elevated H-ferritin expression is due to iron exposure. To answer this question, we stained AS valves with Prussian blue (specific iron staining) and as shown in Figure 8A iron was absent in the highly calcified region. Torti et al. previously demonstrated that inflammatory cytokines upregulate the expression of H-ferritin in the absence of iron [29, 30]. Moreover, inflammation is implicated in the progression of CAVD [1]. Therefore, we performed immunohistochemistry (Figure 9A) and Western blot analysis (Figure 9B) for inflammatory markers, TNF- $\alpha$  and IL1- $\beta$  on human healthy and AS tissue. Importantly, elevated H-ferritin expression corroborated the increased protein level of TNF- $\alpha$  and IL1- $\beta$  in AS tissues as compared to healthy aortic valves (Figure 9).

### **H-ferritin abrogates the expression of inflammatory markers in VIC cells derived from AS tissues**

To test whether ferritin/ferroxidase system has the potential to act against inflammation in CAVD, we treated VIC cells derived from AS tissue with H-ferritin. We found that H-ferritin exposure inhibited the expression of TNF- $\alpha$  and IL1- $\beta$  (Figure 10A). Figure 10B shows the possible mechanisms for the beneficial role of ferritin/ferroxidase in CAVD.

## **Discussion**

This study is the first which highlights the relationship between deranged iron metabolism, a frequent complication of CKD, and valvular calcification. We herein report how cellular iron metabolism may modulate mineralization and osteoblastic transformation of human VIC when cultured in calcification medium. Consistent with previous reports in vascular smooth muscle cells [10, 39] and bioprosthetic tissues [40], we confirm mitigation of the

Author Manuscript

calcification process of VIC through the unifying mechanism of H-ferritin induction via iron, D3T or apo-ferritin [41]. These experiments also confirm previously reported findings that the elevated inorganic phosphate and calcium levels induced the mineralization of VIC [42–44]. We used extracellular calcium level, Alizarin Red S staining, osteocalcin content, ALP staining, and pyrophosphate level as surrogates of VIC transition into osteoblast-like cells and validate the paramount inhibitory role of H-ferritin induction in this process. Importantly, our data suggest that upregulation of intracellular H-ferritin (irrespective of the inducer) prevents nuclear translocation of RUNX2 that is considered the main transcription factor and regulator of osteogenesis [45–47].

Author Manuscript

The high mortality rate of cardiovascular diseases is a major challenge especially in patients with advanced CKD [48, 49]. In fact, patients with CKD with adjusted cardiovascular disease risk factors have about 10–20 fold higher mortality compared to the general population [42, 43]. One of the major contributors to such elevated risk of cardiovascular-related mortality in this group of patients is vascular and valvular calcification [50]. Such valvular abnormalities predispose patients to arrhythmias, infective endocarditis and increased risk of thromboembolism [44, 51–53]. Additionally, numerous studies have demonstrated that elevated Pi level not only is a significant risk factor but also a key regulator of vascular/valvular calcification [10, 24, 39, 54].

Author Manuscript

Ferritin is an abundant and highly conserved three-dimensional protein and plays a major role in intracellular iron handling [55, 56]. The family of ferritins is similar to spherical shells with the capability to sequester and store a large amount of iron in a soluble and bioavailable form. Ferritin has 24 subunits (two types: H, heavy and L, light chain) whose proportions depend on the iron status of the cells, tissue or organ. Only the H-ferritin has ferroxidase activity that can oxidize  $\text{Fe}^{2+}$  to  $\text{Fe}^{3+}$  facilitating the safe incorporation of iron into the shell. Iron is stored in an internal cavity in a ferric oxyhydrophosphate complex [36]. High amounts of iron and phosphate are stored within the core of ferritin [57]. The main functions of ferritin are to depot, sequester and allow availability of iron when needed [55, 58]. In the past decade, our understanding of the role of ferritin and its function has markedly enhanced, and there is significantly more insight into the role of ferritin in the regulation of iron metabolism and homeostasis [27, 56, 59, 60].

Author Manuscript

Expression of H-ferritin is strongly regulated at a translational level by iron via the iron regulatory element/iron regulatory protein machinery. This involves the iron-dependent change in activity of the iron regulatory proteins 1 and 2. In the presence of low iron these proteins bind to the iron-responsive element of mRNA at the 5'UTR of the ferritin transcripts inhibiting their translation, whereas in high iron they lose affinity and translation is derepressed [25]. Importantly, the transcriptional control of the H-ferritin is also linked to oxidative stress and it is affected through the binding of Nrf2/Small Maf protein to conserved antioxidant-responsive element [26]. Induction of H-ferritin is mediated by Nrf2 in response to D3T [61].

Author Manuscript

In our previous studies, we concluded that iron and H-ferritin prevented calcification and osteoblastic transformation of vascular smooth muscle cells induced by the high level of inorganic phosphate [10, 24, 54]. Here we report that H-ferritin and is also a key mediator in

inhibition of VIC calcification. Importantly, our findings suggest that this inhibitory mechanism is an active process whereby primary osteoblast-specific genes are mitigated in response to H-ferritin induction. Given the clinical significance of these findings and the potential of targeting ferritin induction as a novel therapeutic approach, we were encouraged to examine the role of D3T in this context. D3T has a chemopreventive effect in cancer medicine [62]. Using various strategies including H-ferritin RNA silencing, we conclude that D3T mimics the inhibitory properties of iron, apo-ferritin further highlighting the central role of H-ferritin in this process. In addition, these inhibitory effects are also replicated by ceruloplasmin, another protein with ferroxidase activity.

Our findings further cast light on the close relationship between intracellular iron metabolism and osteoblastic activity. Interestingly, Western blot analysis and histological panel for H-ferritin (Figure 7A) revealed significant differences in the expression of intracellular ferritin levels in the AS valve section compared to the AI valve tissue section. Double immunostaining of valve sections (Figure 7B) further corroborated these observations. Moreover, we found that calcified areas of the valves were deficient in ferritin expression (Figure 7B) and such expression was limited to areas that were devoid of mineralization. In contrast, as expected these calcified regions exhibited robust ALP staining (Figure 7B) highlighting their acquired osteoblastic status. These results may suggest an adaptive response where induction of H-ferritin works as a major stratagem to prevent the osteoblastic transition of VIC. Increasing body of evidence highlights the key role of osteogenic transcription factor RUNX2 in cardiovascular calcification in CKD patients [63]. For instance, Raaz et al. investigated the role of RUNX2 as a potential mediator and therapeutic target of aortic fibrosis and aortic stiffening in diabetes mellitus. They found that RUNX2, as a previously unrecognized inducer of vascular fibrosis in the setting of diabetes mellitus, promotes arterial stiffness irrespective of calcification [64]. Furthermore, it has been shown that RUNX2 overexpression induces aortic media fibrosis, increased aortic stiffness, and elevated pulse pressure. These results identify upregulation of RUNX2 as a maladaptive response during injury to the vasculature, uremic milieu, and hyperglycemic conditions [53]. Moreover, we demonstrated that RUNX2 was manifested in the nucleus of AS valve tissue cells with calcification cultured in normal condition compared to AI valve cells, where RUNX2 localized in the cytoplasmic region of the cells (Figure 2C and 2D). These findings demonstrate that nuclear localization of RUNX2 shows the early transformation into osteoblast-like cells of VIC.

RUNX2 and Sox9 were revealed to interact physically in intact cells where Sox9 inhibits the transactivation of RUNX2. In addition, RUNX2 exerts reciprocal inhibition on Sox9 activity. Sox9 was shown to induce a dose-dependent degradation of RUNX2 [13–16]. In our studies, we also found a reciprocal and counter-regulatory interaction between RUNX2 and Sox9. In calcifying condition nuclear Sox9 level in VIC was decreased, conversely, RUNX2 level was increased. Accordingly, cells of stenotic aortic valve with calcification exhibited higher level of nuclear RUNX2 and lower level of Sox9 as compared to isolated aortic valve with insufficiency. Importantly, treatment of VIC with iron, apo-ferritin and D3T enhanced the presence of Sox9 in nucleus and maintained nuclear RUNX2 at low level. These findings indicate that one of the targets for ferritin (iron and D3T) to inhibit mineralization of VIC is mediated by modulation of Sox9 and subsequently RUNX2. Alternatively, inhibition of

phosphate uptake (Figure 4A) via decreasing the expression of Pit1 and Pit2 channels (Figure 4C and D) by ferritin may also contribute to the attenuation of RUNX2 nuclear translocation, thereby preventing osteoblastic phenotype transition, the appearance of osteoblastic phenotype, as reflected by ALP, osteocalcin expression and the development of the hydroxyapatite crystals. The paramount role of ferroxidase activity of ferritin is confirmed by enhanced RUNX2 nuclear translocation resulting in osteoblastic transformation of VIC after silencing the H-ferritin gene (Supplementary Figure V). Accordingly, exogenous H-ferritin decreased the expression of Pit1 channel and subsequently lowered phosphate uptake in VIC (Figure 4E and Supplementary Figure VI. C). Although lysosomal localization of ferritin/ferroxidase induced by iron or D3T is demonstrated, some caveat is acknowledged. The mechanism by which H-ferritin/ferroxidase activity alters the activity of RUNX2 and its subcellular localization, and the expression of Pit1 and Pit2 channels have not been explored in our studies.

Christian de Duve in 1955 described for the first time that lysosomes are membrane-bound organelles. They have a single-bilayer lipid membrane which limits their acidic lumen. Lysosomes contain several types of hydrolases that are devoted to the degradation of specific substrates. The lysosomal membrane-proteins are involved the transport of substances into and out of the lumen, acidification of the lysosomal lumen, and fusion of the lysosome with other cellular structures [65]. Importantly, Mancias et al. revealed that nuclear receptor coactivator 4 is required for delivery of ferritin to lysosomes [66] and alternative lysosomal transport has also been described [67]. Therefore, we tested whether the excess intracellular phosphate could be depleted by ferritin and transported into the lysosome. Ferritin has a hollow internal cavity for storing iron and phosphate (2250 and 380 atoms, respectively). We demonstrate that H-ferritin and the main protein of the lysosome LAMP1 could interact, and such interaction may play a crucial role in the general homeostasis of the cells including phosphate level (Figure 4).

Pyrophosphate level in plasma is an endogenous inhibitor of vascular calcification, which is reduced in end-stage renal disease and correlates inversely with arterial calcification [68]. The three most closely related ENPPs - ENPP1, ENPP2 and ENPP3 - all generate extracellular PPI from ATP [69]. However, ENPPs differ in substrate specificities. The current convention based upon human genetics of generalized arterial calcification of infancy (GACI) [70, 71] is that ENPP1 may be the major source of NTP-dependent PPI during vertebrate development. The importance of ENPPs indicated by ENPP1 genetic deficiency causes GACI, which is a lethal cardiovascular calcification disease [71]. In our study, we showed decreased ENPP2 expression accompanied by lower PPI generation under calcification condition. Exposure of cells to iron, Apo-ferritin D3T and H-ferritin upregulated ENPP2 and subsequently enhanced the production of PPI (Figure 6). A drop in PPI level occurred after silencing the expression of H-ferritin in VIC exposed to iron. These data suggest that ferritin may also act via ENPP2 and PPI to control mineralization of VIC.

Mendelian randomization studies [72–74] have highlighted that lipoprotein(a) [Lp(a)] was associated with calcific aortic valve disease (CAVD). Lp(a) transports oxidized phospholipids with a high content in lysophosphatidylcholine. ENPP2 is present in the Lp(a) fraction in circulation and also expressed by VICs in CAVD. ENPP2 acts on

lysophosphatidylcholine and catalyzes the extracellular production of lysophosphatidic acid, a pro-osteogenic agonist likely via the LPA1 receptor [75]. In our studies H-ferritin enhanced the biogenesis of PPI via increasing the expression of ENPP2 and decreasing ALP level, the major enzyme degrading PPI. The control of ENPP2 activity to generate PPI versus lysophosphatidic acid may represent a key regulatory mechanism mediating the anti-calcification actions by H-ferritin (Figure 10C).

Additionally, we found that H-ferritin is highly expressed in VIC of AS valve, and the level increases toward the calcific core. The relative dominance of H-ferritin over ALP in the intact area of valves might indicate an adaptive response to the calcifying milieu in CAVD. What prompts and triggers expression of H-ferritin in this context remains to be fully elucidated. The pathogenesis of CAVD is complex, and its manifestations appear after long-term exposure to risk factors, leading to altered activation of signaling pathways important in the development of valves and bone [76].

NHLBI working group demonstrated that CAVD is an active and well-regulated inflammatory disease, however specific pathobiological mechanisms are not fully understood [1]. It was previously shown that inflammatory cytokines induce H-ferritin expression [29, 30]. In the present study, we also found that elevation H-ferritin expression was accompanied by inflammatory markers as TNF- $\alpha$  and IL1- $\beta$  in AS tissues without the accumulation of iron (Figure 9A–B). Importantly, H-ferritin decreased the expression of TNF- $\alpha$  and IL1- $\beta$  in VIC derived from human AS valve (Figure 10A). These data may suggest a potential role of H-ferritin in controlling inflammation in CAVD (Figure 10B).

In conclusion, we report for the first time a novel role of ferritin/ferroxidase system in the context of human VIC mineralization and transdifferentiation into osteoblast-like cells. The chemical treatment of D3T and its inhibitory role via H-ferritin induction may be a potential preventive measure in cardiovascular calcification. Furthermore, these findings will provide a novel platform for more in-depth research into the process of physiological and pathological bone formation and identify previously unknown targets to mitigate the detrimental consequences of cardiovascular calcification in CKD.

## Supplementary Material

Refer to Web version on PubMed Central for supplementary material.

## Acknowledgment

We thank our colleagues Gerardo Alvarado, PhD, László Herczeg, PhD and Zsolt Combi for their excellent technical assistance.

### Sources of founding

The research group is supported by the Hungarian Academy of Sciences (11003). This research was supported by Hungarian Government grant, OTKA-K112333 (J.B.) and by the GINOP-2.3.2-15-2016-00043 (IRONHEART); and EFOP-3.6.2-16-2017-00006 project, NIH-NHLBI grant (K08HL140294 to A.Z.). L.P. was supported by János Apáczai-Csere fellowship (TÁMOP 4.2.4.A/2-11/1-2012-0001). The project is co-financed by the European Union and the European Regional Development Fund.

## Abbreviations:

<b>CAVD</b>	Calcific aortic valve disease
<b>VIC</b>	Valvular Interstitial Cells
<b>AI</b>	isolated aortic valve with insufficiency
<b>AS</b>	stenotic aortic valve with calcification
<b>pVIC</b>	porcine VIC
<b>RUNX2</b>	Runt-related transcription factor 2
<b>Sox9</b>	SRY (sex determining region Y)-box 9
<b>AF</b>	Apo-ferritin
<b>ENPP2</b>	ectonucleotide pyrophosphatase/phosphodiesterase family member 2
<b>ANK1</b>	Ankyrin G1
<b>PPi</b>	pyrophosphate
<b>AFT</b>	apo-ferritin
<b>HFT</b>	H-ferritin
<b>HFT222</b>	Mutant H-ferritin222
<b>D3T</b>	3H-1, 2-dithiole-3-thione
<b>IHC</b>	Immunohistochemistry
<b>TNF-<math>\alpha</math></b>	Tumor necrosis factor-alpha
<b>IL1-<math>\beta</math></b>	Interleukin 1-beta

## References

1. Rajamannan NM, Evans FJ, Aikawa E, Grande-Allen KJ, Demer LL, Heistad DD, Simmons CA, Masters KS, Mathieu P, O'Brien KD, Schoen FJ, Towler DA, Yoganathan AP, Otto CM. Calcific aortic valve disease: not simply a degenerative process: A review and agenda for research from the National Heart and Lung and Blood Institute Aortic Stenosis Working Group. Executive summary: Calcific aortic valve disease-2011 update. *Circulation* 2011; 124: 1783–1791. [PubMed: 22007101]
2. Mohler ER, 3rd, Gannon F, Reynolds C, Zimmerman R, Keane MG, Kaplan FS. Bone formation and inflammation in cardiac valves. *Circulation* 2001; 103: 1522–1528. [PubMed: 11257079]
3. Mazzone A, Epistolato MC, De Caterina R, Storti S, Vittorini S, Sbrana S, Gianetti J, Bevilacqua S, Glauber M, Biagini A, Tanganelli P. Neoangiogenesis, T-lymphocyte infiltration, and heat shock protein-60 are biological hallmarks of an immunomediated inflammatory process in end-stage calcified aortic valve stenosis. *Journal of the American College of Cardiology* 2004; 43: 1670–1676. [PubMed: 15120829]
4. Freeman RV, Otto CM. Spectrum of calcific aortic valve disease: pathogenesis, disease progression, and treatment strategies. *Circulation* 2005; 111: 3316–3326. [PubMed: 15967862]

5. Dweck MR, Boon NA, Newby DE. Calcific Aortic Stenosis: A Disease of the Valve and the Myocardium. *Journal of the American College of Cardiology* 2012; 60: 1854–1863. [PubMed: 23062541]
6. Yutzey KE, Demer LL, Body SC, Huggins GS, Towler DA, Giachelli CM, Hofmann-Bowman MA, Mortlock DP, Rogers MB, Sadeghi MM, Aikawa E. Calcific aortic valve disease: a consensus summary from the Alliance of Investigators on Calcific Aortic Valve Disease. *Arterioscler Thromb Vasc Biol* 2014; 34: 2387–2393. [PubMed: 25189570]
7. Lusis AJ, Mar R, Pajukanta P. Genetics of atherosclerosis. *Annu Rev Genomics Hum Genet* 2004; 5: 189–218. [PubMed: 15485348]
8. Mohler ER, 3rd, Mechanisms of aortic valve calcification. *Am J Cardiol* 2004; 94: 1396–1402, a1396. [PubMed: 15566910]
9. Speer MY, Giachelli CM. Regulation of cardiovascular calcification. *Cardiovasc Pathol* 2004; 13: 63–70. [PubMed: 15033154]
10. Zarjou A, Jeney V, Arosio P, Poli M, Antal-Szalms P, Agarwal A, Balla G, Balla J. Ferritin prevents calcification and osteoblastic differentiation of vascular smooth muscle cells. *Journal of the American Society of Nephrology : JASN* 2009; 20: 1254–1263. [PubMed: 19423691]
11. Rajamannan NM, Subramaniam M, Rickard D, Stock SR, Donovan J, Springett M, Orszulak T, Fullerton DA, Tajik AJ, Bonow RO, Spelsberg T. Human aortic valve calcification is associated with an osteoblast phenotype. *Circulation* 2003; 107: 2181–2184. [PubMed: 12719282]
12. Caira FC, Stock SR, Gleason TG, McGee EC, Huang J, Bonow RO, Spelsberg TC, McCarthy PM, Rahimtoola SH, Rajamannan NM. Human degenerative valve disease is associated with up-regulation of low-density lipoprotein receptor-related protein 5 receptor-mediated bone formation. *J Am Coll Cardiol* 2006; 47: 1707–1712. [PubMed: 16631011]
13. Lincoln J, Kist R, Scherer G, Yutzey KE. Sox9 is required for precursor cell expansion and extracellular matrix organization during mouse heart valve development. *Developmental biology* 2007; 305: 120–132. [PubMed: 17350610]
14. Peacock JD, Levay AK, Gillaspie DB, Tao G, Lincoln J. Reduced Sox9 function promotes heart valve calcification phenotypes in vivo. *Circulation research* 2010; 106: 712–719. [PubMed: 20056916]
15. Huk DJ, Austin BF, Horne TE, Hinton RB, Ray WC, Heistad DD, Lincoln J. Valve Endothelial Cell-Derived Tgfbeta1 Signaling Promotes Nuclear Localization of Sox9 in Interstitial Cells Associated With Attenuated Calcification. *Arterioscler Thromb Vasc Biol* 2016; 36: 328–338. [PubMed: 26634652]
16. Cheng A, Genever PG. SOX9 determines RUNX2 transactivity by directing intracellular degradation. *J Bone Miner Res* 2010; 25: 2680–2689. [PubMed: 20593410]
17. Hruska KA, Mathew S, Lund R, Qiu P, Pratt R. Hyperphosphatemia of chronic kidney disease. *Kidney Int* 2008; 74: 148–157. [PubMed: 18449174]
18. Giachelli CM. The emerging role of phosphate in vascular calcification. *Kidney Int* 2009; 75: 890–897. [PubMed: 19145240]
19. Adeney KL, Siscovick DS, Ix JH, Seliger SL, Shlipak MG, Jenny NS, Kestenbaum BR. Association of serum phosphate with vascular and valvular calcification in moderate CKD. *J Am Soc Nephrol* 2009; 20: 381–387. [PubMed: 19073826]
20. Li X, Yang HY, Giachelli CM. Role of the sodium-dependent phosphate cotransporter, Pit-1, in vascular smooth muscle cell calcification. *Circ Res* 2006; 98: 905–912. [PubMed: 16527991]
21. Crouthamel MH, Lau WL, Leaf EM, Chavkin NW, Wallingford MC, Peterson DF, Li X, Liu Y, Chin MT, Levi M, Giachelli CM. Sodium-dependent phosphate cotransporters and phosphate-induced calcification of vascular smooth muscle cells: redundant roles for PiT-1 and PiT-2. *Arterioscler Thromb Vasc Biol* 2013; 33: 2625–2632. [PubMed: 23968976]
22. Jansen S, Perrakis A, Ulens C, Winkler C, Andries M, Joosten RP, Van Acker M, Luyten FP, Moolenaar WH, Bollen M. Structure of NPP1, an ectonucleotide pyrophosphatase/phosphodiesterase involved in tissue calcification. *Structure* 2012; 20: 1948–1959. [PubMed: 23041369]
23. Mitton-Fitzgerald E, Gohr CM, Bettendorf B, Rosenthal AK. The Role of ANK in Calcium Pyrophosphate Deposition Disease. *Curr Rheumatol Rep* 2016; 18: 25. [PubMed: 27032788]

24. Zarjou A, Jeney V, Arosio P, Poli M, Zavaczki E, Balla G, Balla J. Ferritin ferroxidase activity: a potent inhibitor of osteogenesis. *Journal of bone and mineral research : the official journal of the American Society for Bone and Mineral Research* 2010; 25: 164–172.
25. Kuhn LC. Iron regulatory proteins and their role in controlling iron metabolism. *Metallomics* 2015; 7: 232–243. [PubMed: 25306858]
26. Theil EC, Behera RK, Tosha T. Ferritins for Chemistry and for Life. *Coord Chem Rev* 2013; 257: 579–586. [PubMed: 23470857]
27. Pietsch EC, Chan JY, Torti FM, Torti SV. Nrf2 mediates the induction of ferritin H in response to xenobiotics and cancer chemopreventive dithiolethiones. *Journal of Biological Chemistry* 2003; 278: 2361–2369. [PubMed: 12435735]
28. Becs G, Zarjou A, Agarwal A, Kovacs KE, Becs A, Nyitrai M, Balogh E, Banyai E, Eaton JW, Arosio P, Poli M, Jeney V, Balla J, Balla G. Pharmacological induction of ferritin prevents osteoblastic transformation of smooth muscle cells. *J Cell Mol Med* 2016; 20: 217–230. [PubMed: 26499096]
29. Torti SV, Kwak EL, Miller SC, Miller LL, Ringold GM, Myambo KB, Young AP, Torti FM. The molecular cloning and characterization of murine ferritin heavy chain, a tumor necrosis factor-inducible gene. *J Biol Chem* 1988; 263: 12638–12644. [PubMed: 3410854]
30. Tsuji Y, Miller LL, Miller SC, Torti SV, Torti FM. Tumor necrosis factor-alpha and interleukin 1-alpha regulate transferrin receptor in human diploid fibroblasts. Relationship to the induction of ferritin heavy chain. *J Biol Chem* 1991; 266: 7257–7261. [PubMed: 2016326]
31. Gould RA, Butcher JT. Isolation of valvular endothelial cells. *J Vis Exp* 2010.
32. Komori T, Yagi H, Nomura S, et al. Targeted disruption of Cbfa1 results in a complete lack of bone formation owing to maturational arrest of osteoblasts. *Cell* 1997; 89: 755–764. [PubMed: 9182763]
33. Steitz SA, Speer MY, Curinga G, Yang HY, Haynes P, Aebersold R, Schinke T, Karsenty G, Giachelli CM. Smooth muscle cell phenotypic transition associated with calcification: upregulation of Cbfa1 and downregulation of smooth muscle lineage markers. *Circ Res* 2001; 89: 1147–1154. [PubMed: 11739279]
34. Jono S, McKee MD, Murry CE, Shioi A, Nishizawa Y, Mori K, Morii H, Giachelli CM. Phosphate regulation of vascular smooth muscle cell calcification. *Circ Res* 2000; 87: E10–17. [PubMed: 11009570]
35. Fujita T, Izumo N, Fukuyama R, Meguro T, Nakamuta H, Kohno T, Koida M. Phosphate provides an extracellular signal that drives nuclear export of Runx2/Cbfa1 in bone cells. *Biochem Biophys Res Commun* 2001; 280: 348–352. [PubMed: 11162521]
36. de Silva D, Guo JH, Aust SD. Relationship between iron and phosphate in mammalian ferritins. *Arch Biochem Biophys* 1993; 303: 451–455. [PubMed: 8512327]
37. Fleisch H, Bisaz S. Mechanism of Calcification: Inhibitory Role of Pyrophosphate. *Nature* 1962; 195: 911.
38. Terkeltaub RA. Inorganic pyrophosphate generation and disposition in pathophysiology. *Am J Physiol Cell Physiol* 2001; 281: C1–c11. [PubMed: 11401820]
39. Becs G, Zarjou A, Agarwal A, Kovacs K, Becs d, Nyitrai M, Balogh E, Banyai E, Eaton JW, Arosio P, Poli M, Jeney V, Balla J, Balla G. Pharmacological induction of ferritin prevents osteoblastic transformation of smooth muscle cells. *Journal of Cellular and Molecular Medicine* 2016; 20: 217–230. [PubMed: 26499096]
40. Carpentier SM, Carpentier AF, Chen L, Shen M, Quintero LJ, Witzel TH. Calcium mitigation in bioprosthetic tissues by iron pretreatment: The challenge of iron leaching. *The Annals of Thoracic Surgery* 1995; 60.
41. Primiano T, Kensler TW, Kuppasamy P, Zweier JL, Sutter TR. Induction of hepatic heme oxygenase-1 and ferritin in rats by cancer chemopreventive dithiolethiones. *Carcinogenesis* 1996; 17: 2291–2296. [PubMed: 8968040]
42. Mathieu P, Voisine P, Pepin A, Shetty R, Savard N, Dagenais F. Calcification of human valve interstitial cells is dependent on alkaline phosphatase activity. *J Heart Valve Dis* 2005; 14: 353–357. [PubMed: 15974530]

43. Block GA. Prevalence and clinical consequences of elevated Ca x P product in hemodialysis patients. *Clin Nephrol* 2000; 54: 318–324. [PubMed: 11076108]
44. London GM, Pannier B, Marchais SJ, Guerin aP. Calcification of the aortic valve in the dialyzed patient. *Journal of the American Society of Nephrology : JASN* 2000; 11: 778–783. [PubMed: 10752538]
45. Komori T, Yagi H, Nomura S, et al. Targeted Disruption of Cbfa1 Results in a Complete Lack of Bone Formation owing to Maturational Arrest of Osteoblasts. *Cell* 1997; 89: 755–764. [PubMed: 9182763]
46. Speer MY, Li X, Hiremath PG, Giachelli CM. Runx2/Cbfa1, but not loss of myocardin, is required for smooth muscle cell lineage reprogramming toward osteochondrogenesis. *Journal of Cellular Biochemistry* 2010; 110: 935–947. [PubMed: 20564193]
47. Steitz SA, Speer MY, Curinga G, Yang HY, Haynes P, Aebbersold R, Schinke T, Karsenty G, Giachelli CM. Smooth Muscle Cell Phenotypic Transition Associated With Calcification: Upregulation of Cbfa1 and Downregulation of Smooth Muscle Lineage Markers. *Circulation Research* 2001; 89: 1147–1154. [PubMed: 11739279]
48. Weir MR. Recognizing the link between chronic kidney disease and cardiovascular disease. *The American journal of managed care* 2011; 17 Suppl 1: S396–402. [PubMed: 22214474]
49. Kumar S Why do young people with chronic kidney disease die early? *World Journal of Nephrology* 2014; 3: 143. [PubMed: 25374808]
50. Moradi H, Sica DA, Kalantar-Zadeh K. Cardiovascular burden associated with uremic toxins in patients with chronic kidney disease. *American Journal of Nephrology* 2013; 38: 136–148. [PubMed: 23941724]
51. Maher ER, Young G, Smyth-Walsh B, Pugh S, Curtis JR. Aortic and mitral valve calcification in patients with end-stage renal disease. *Lancet* 1987; 2: 875–877. [PubMed: 2889080]
52. Wang AYM. Cardiac Valve Calcification as an Important Predictor for All-Cause Mortality and Cardiovascular Mortality in Long-Term Peritoneal Dialysis Patients: A Prospective Study. *Journal of the American Society of Nephrology* 2003; 14: 159–168. [PubMed: 12506148]
53. Di Iorio BR, Bortone S, Piscopo C, Grimaldi P, Cucciniello E, D'Avanzo E, Mondillo F, Cillo N, Bellizzi V. Cardiac vascular calcification and QT interval in ESRD patients: is there a link? *Blood Purif* 2006; 24: 451–459. [PubMed: 16940716]
54. Arosio P, Ingrassia R, Cavadini P. Ferritins: A family of molecules for iron storage, antioxidation and more. *Biochimica et Biophysica Acta - General Subjects* 2009; 1790: 589–599.
55. Finazzi D, Arosio P. Biology of ferritin in mammals: an update on iron storage, oxidative damage and neurodegeneration. *Archives of toxicology* 2014; 88: 1787–1802. [PubMed: 25119494]
56. Coffman LG, Parsonage D, D'Agostino R, Torti FM, Torti SV. Regulatory effects of ferritin on angiogenesis. *Proceedings of the National Academy of Sciences* 2009; 106: 570–575.
57. Juan SH, Aust SD. Iron and phosphate content of rat ferritin heteropolymers. *Arch Biochem Biophys* 1998; 357: 293–298. [PubMed: 9735170]
58. Alkhateeb AA, Connor JR. Nuclear ferritin: A new role for ferritin in cell biology. *Biochimica et Biophysica Acta - General Subjects* 2010; 1800: 793–797.
59. Alani H Cardiovascular co-morbidity in chronic kidney disease: Current knowledge and future research needs. *World Journal of Nephrology* 2014; 3: 156. [PubMed: 25374809]
60. Zarjou A, Bolisetty S, Joseph R, Traylor A, Apostolov EO, Arosio P, Balla J, Verlander J, Darshan D, Kuhn LC, Agarwal A. Proximal tubule h-ferritin mediates iron trafficking in acute kidney injury. *Journal of Clinical Investigation* 2013; 123: 4423–4434. [PubMed: 24018561]
61. Pietsch EC, Chan JY, Torti FM, Torti SV. Nrf2 mediates the induction of ferritin H in response to xenobiotics and cancer chemopreventive dithiolethiones. *J Biol Chem* 2003; 278: 2361–2369. [PubMed: 12435735]
62. Zhang Y, Munday R. Dithiolethiones for Cancer Chemoprevention : Where Do We. 2009; 7: 3470–3479.
63. Hosen MJ, Coucke PJa. Perturbation of specific pro-mineralizing signalling pathways in human and murine pseudoxanthoma elasticum. *Orphanet journal of rare diseases* 2014; 9: 66. [PubMed: 24775865]

64. Raaz U, Schellinger IN, Chernogubova E, et al. Transcription factor Runx2 promotes aortic fibrosis and stiffness in type 2 diabetes mellitus. *Circulation Research* 2015; 117: 513–524. [PubMed: 26208651]
65. Saftig P, Klumperman J. Lysosome biogenesis and lysosomal membrane proteins: trafficking meets function. *Nature Reviews Molecular Cell Biology* 2009; 10: 623–635. [PubMed: 19672277]
66. Mancias JD, Wang X, Gygi SP, Harper JW, Kimmelman AC. Quantitative proteomics identifies NCOA4 as the cargo receptor mediating ferritinophagy. *Nature* 2014; 509: 105–109. [PubMed: 24695223]
67. Goodwin JM, Dowdle WE, DeJesus R, Wang Z, Bergman P, Kobylarz M, Lindeman A, Xavier RJ, McAllister G, Nyfeler B, Hoffman G, Murphy LO. Autophagy-Independent Lysosomal Targeting Regulated by ULK1/2-FIP200 and ATG9. *Cell Rep* 2017; 20: 2341–2356. [PubMed: 28877469]
68. Lomashvili KA, Narisawa S, Millan JL, O'Neill WC. Vascular calcification is dependent on plasma levels of pyrophosphate. *Kidney Int* 2014; 85: 1351–1356. [PubMed: 24717293]
69. Prosdocimo DA, Douglas DC, Romani AM, O'Neill WC, Dubyak GR. Autocrine ATP release coupled to extracellular pyrophosphate accumulation in vascular smooth muscle cells. *Am J Physiol Cell Physiol* 2009; 296: C828–839. [PubMed: 19193865]
70. Rutsch F, Ruf N, Vaingankar S, et al. Mutations in ENPP1 are associated with 'idiopathic' infantile arterial calcification. *Nat Genet* 2003; 34: 379–381. [PubMed: 12881724]
71. Nitschke Y, Baujat G, Botschen U, et al. Generalized arterial calcification of infancy and pseudoxanthoma elasticum can be caused by mutations in either ENPP1 or ABCC6. *Am J Hum Genet* 2012; 90: 25–39. [PubMed: 22209248]
72. Thanassoulis G, Campbell CY, Owens DS, et al. Genetic associations with valvular calcification and aortic stenosis. *N Engl J Med* 2013; 368: 503–512. [PubMed: 23388002]
73. Kamstrup PR, Tybjaerg-Hansen A, Nordestgaard BG. Elevated lipoprotein(a) and risk of aortic valve stenosis in the general population. *J Am Coll Cardiol* 2014; 63: 470–477. [PubMed: 24161338]
74. Arsenault BJ, Boekholdt SM, Dube MP, Rheaume E, Wareham NJ, Khaw KT, Sandhu MS, Tardif JC. Lipoprotein(a) levels, genotype, and incident aortic valve stenosis: a prospective Mendelian randomization study and replication in a case-control cohort. *Circ Cardiovasc Genet* 2014; 7: 304–310. [PubMed: 24704946]
75. Mathieu P, Arsenault BJ, Boulanger MC, Bosse Y, Koschinsky ML. Pathobiology of Lp(a) in calcific aortic valve disease. *Expert Rev Cardiovasc Ther* 2017; 15: 797–807. [PubMed: 28816078]
76. Dutta P, Lincoln J. Calcific Aortic Valve Disease: a Developmental Biology Perspective. *Curr Cardiol Rep* 2018; 20: 21. [PubMed: 29520694]

### Highlights

1. H-ferritin induces by iron and 3H-1, 2-dithiole-3-thione inhibits mineralization and osteoblastic differentiation of human valvular interstitial cells.
2. H-ferritin enhances nuclear localization of transcription factor Sox9, and as a reciprocal effect it reduces nuclear accumulation of RUNX2.
3. H-ferritin inhibits cellular phosphate uptake and lysosomal phosphate accumulation via decreasing the expression of phosphate channels and localization of lysosomal H-ferritin with high phosphate binding capacity, as well as enhances pyrophosphate generation via up-regulating ENPP2.
4. Histological analysis of stenotic aortic valve revealed high expression of H-ferritin and its relative dominance over ALP in the intact non-calcified regions.
5. H-ferritin decreases the expression of inflammatory markers (TNF- $\alpha$  and IL1- $\beta$ ) in VIC derived from human AS valve.

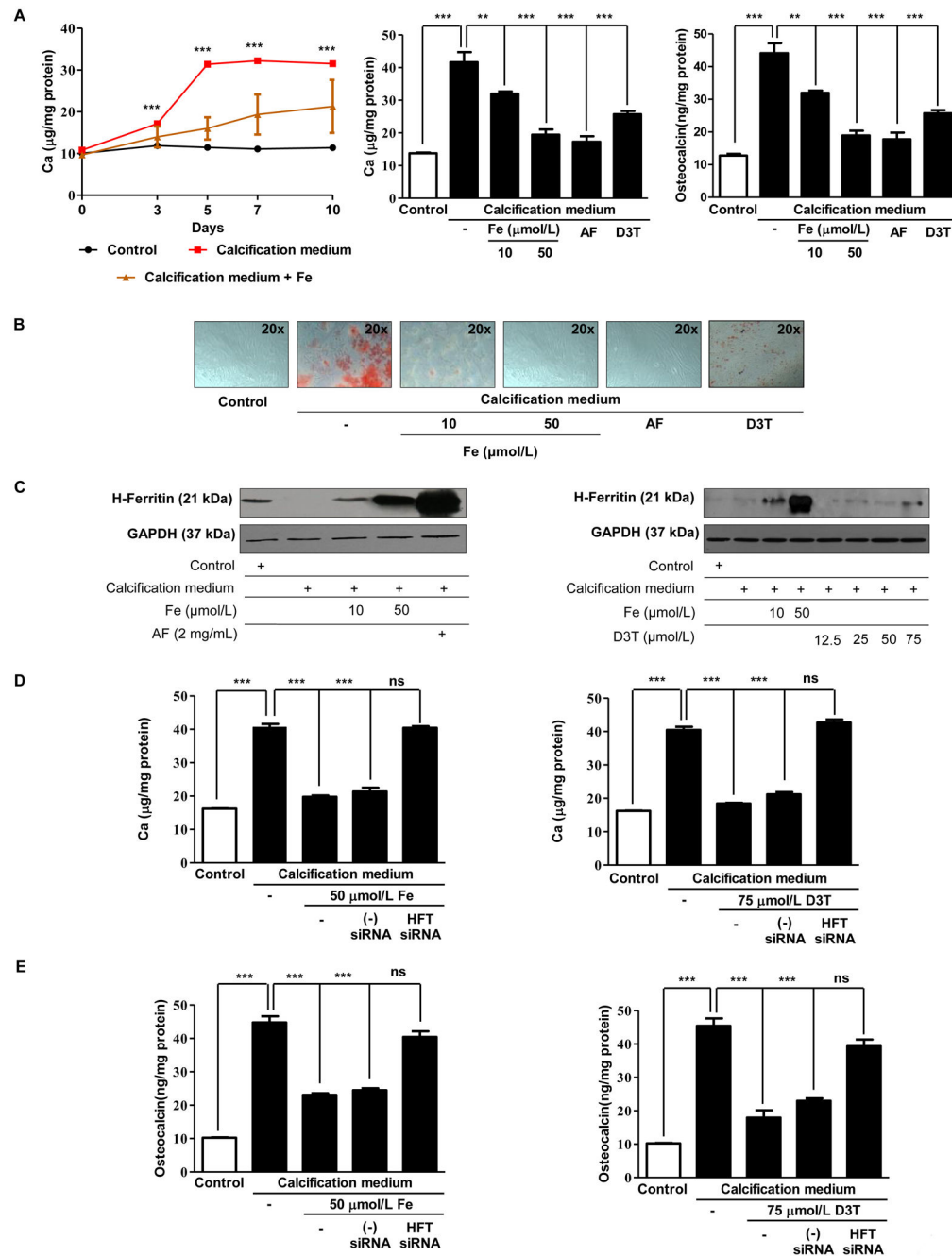


**Figure 1. Calcification of valvular interstitial cells is inhibited by iron, D3T, and apo-ferritin**

A) VIC was cultured in growth medium or calcification medium in the presence or absence of 10, 50  $\mu\text{mol}/\text{L}$  iron (Ammonium iron (III) citrate) and 2 mg/mL apo-ferritin. Calcium contents of the cells were measured after 0, 3, 5, 7 and ten days and normalized to protein content of the cells (left panel). Calcium content and representative images of Alizarin Red staining (Figure 1B) are shown. Figure 1 (middle panel) Calcium and Figure 1 (right panel) osteocalcin content of the cells were measured after five days incubation. Osteocalcin and calcium level were normalized to protein concentration of cells. C) Representative Western blot shows expression of H-ferritin and GAPDH of cells treated as described above. 60%

confluence of VIC was transfected with siRNA specific to H-ferritin or negative control siRNA 24 hours before the experiment. Cells were cultured in growth medium or calcification medium in the presence or absence of iron or D3T for five days. D) Calcium deposition, E) Osteocalcin level was measured. Graphs analyzed by One Way ANOVA, Bonferroni's Multiple Comparison Test and show mean  $\pm$ SEM of three independent experiments. Not significant (ns), \*\*  $P < 0.001$ , \*\*\*  $P < 0.0001$ .

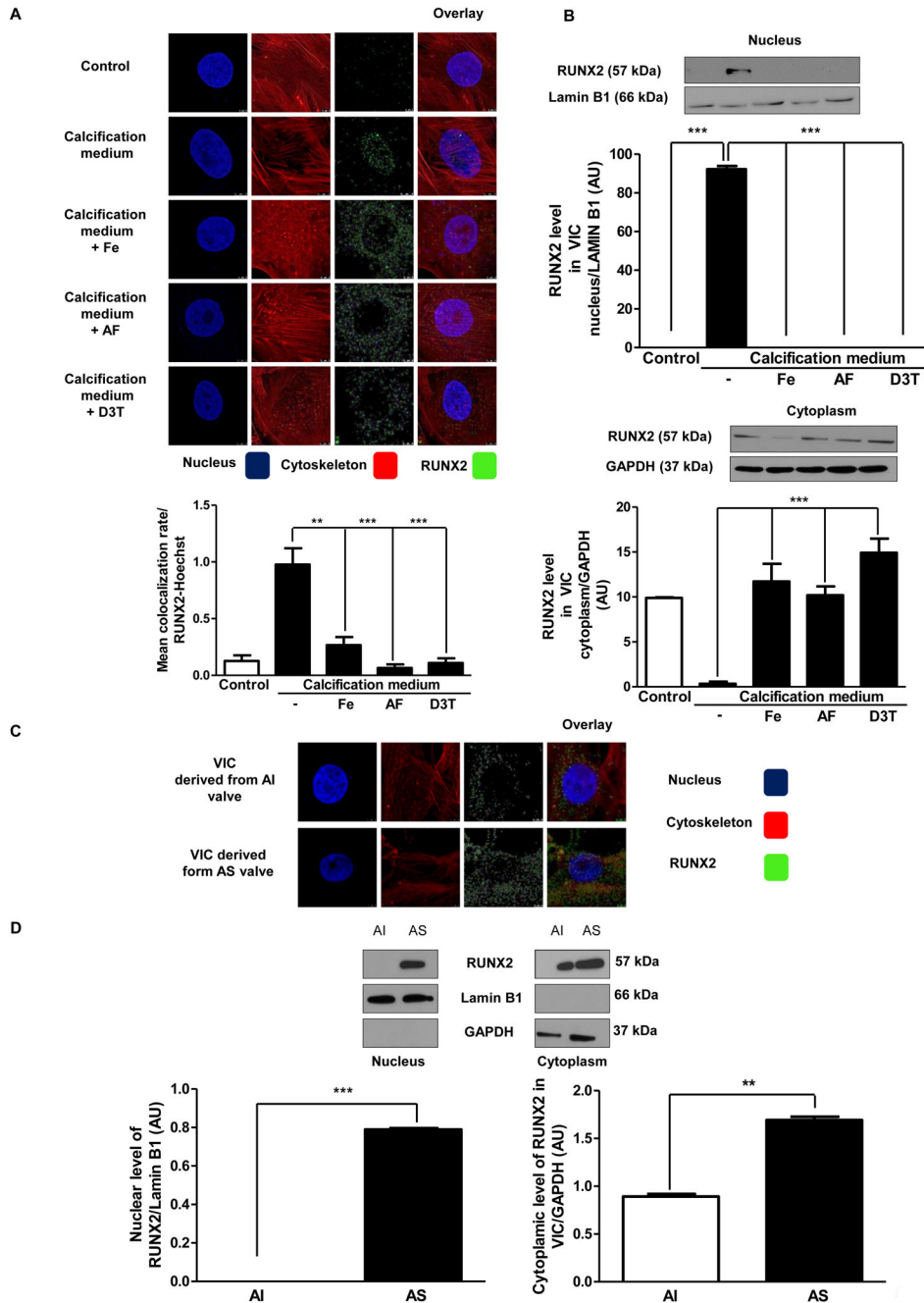


**Figure 2. Nuclear translocation of RUNX2 is prevented by iron, apo-ferritin and D3T**  
 A) VIC was cultured with 50  $\mu\text{mol/L}$  iron (Ammonium iron(III) citrate), 2 mg/mL apo-ferritin, 75  $\mu\text{mol/L}$  D3T added into the calcification medium and localization of transcription factor RUNX2 was examined (green). Colocalization of RUNX2 and Hoechst was measured. B) Representative Western blot of RUNX2 from isolated nucleus and cytoplasm of VIC. Samples were normalized for GAPDH and Lamin B1. C) RUNX2 immunostainings of VIC derived from AI or AS valves are shown. Brightness was adjusted by 40%. D) RUNX2 protein level isolated from AI and AS tissues. Results were normalized to Lamin B1 and GAPDH. Images were obtained employing immunofluorescence-confocal STED

nanoscopy. Representative staining is shown from at least three independent experiments. Results were analyzed by One Way ANOVA, Bonferroni's Multiple Comparison Test (Figure 2A–C) and Paired t-test (Figure 2D) and are shown as mean values  $\pm$  SEM of at least three independent experiments. \*\*P < 0.001; \*\*\*P < 0.0001.

Author Manuscript

Author Manuscript

Author Manuscript

Author Manuscript

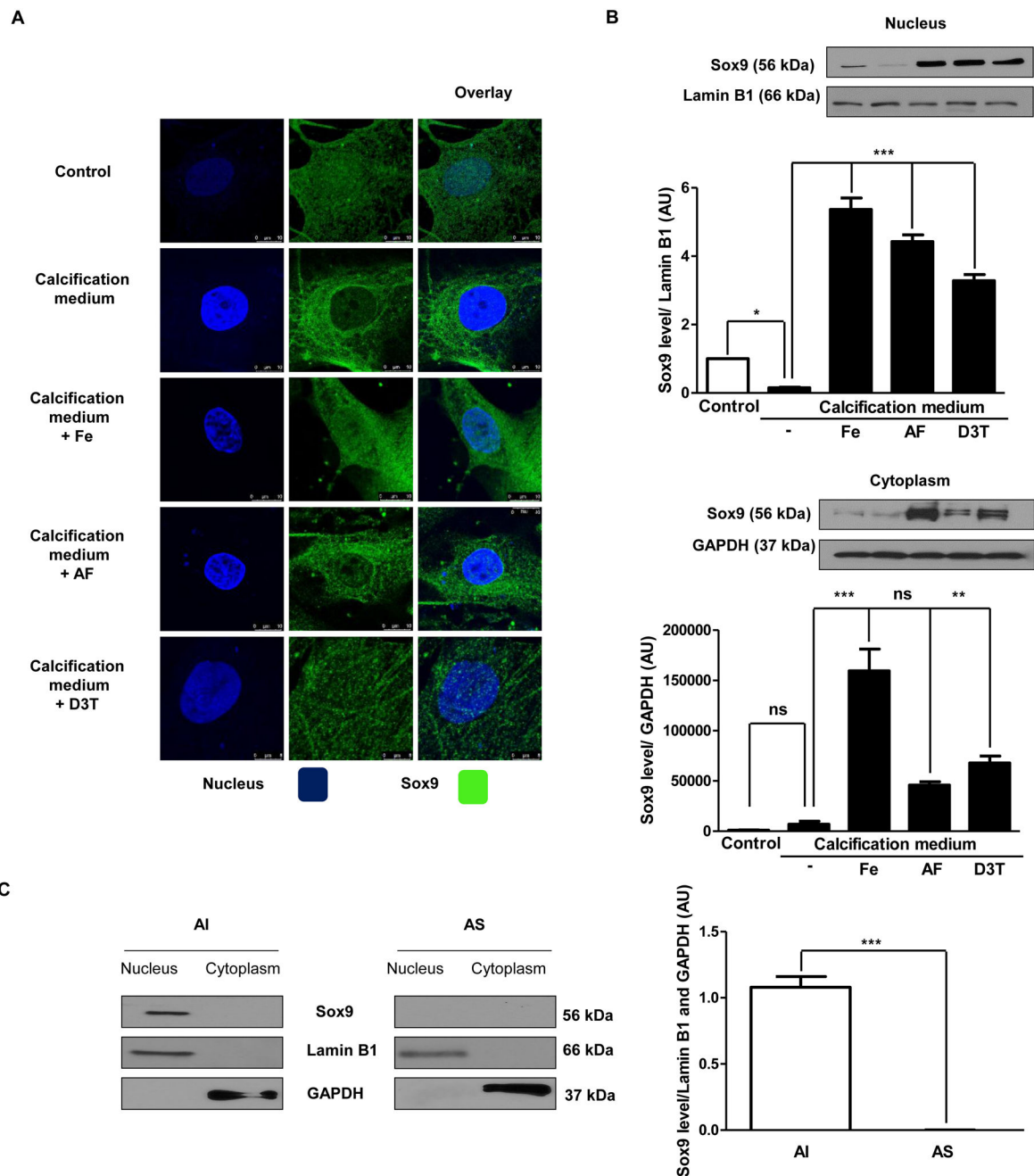


### Figure 3. Calcifying milieu inhibits Sox9 nuclear localization

VIC was cultured in growth medium or calcification medium in the presence or absence of 10, 50  $\mu\text{mol/L}$  iron (Ammonium iron (III) citrate) and 2 mg/mL apo-ferritin. A) Localization of Sox9 was shown (stained green) by immunostaining. Images were obtained employing immunofluorescence-confocal STED nanoscopy. B) Sox9 protein expression from isolated nucleus and cytoplasm fraction also shown. Results were normalized to Lamin B1 and GAPDH. C) Co-localization of Sox9 in VIC. Representative staining is shown from at least three independent experiments. Data were analyzed by One Way ANOVA, Bonferroni's

Multiple Comparison Test (Figure 3A–B)) and Paired t-test (Figure 3C) and shows the average of three separate experiments performed in duplicate. \*\* P<0,001; \*\*\*P < 0.0001.

Author Manuscript

Author Manuscript

Author Manuscript

Author Manuscript

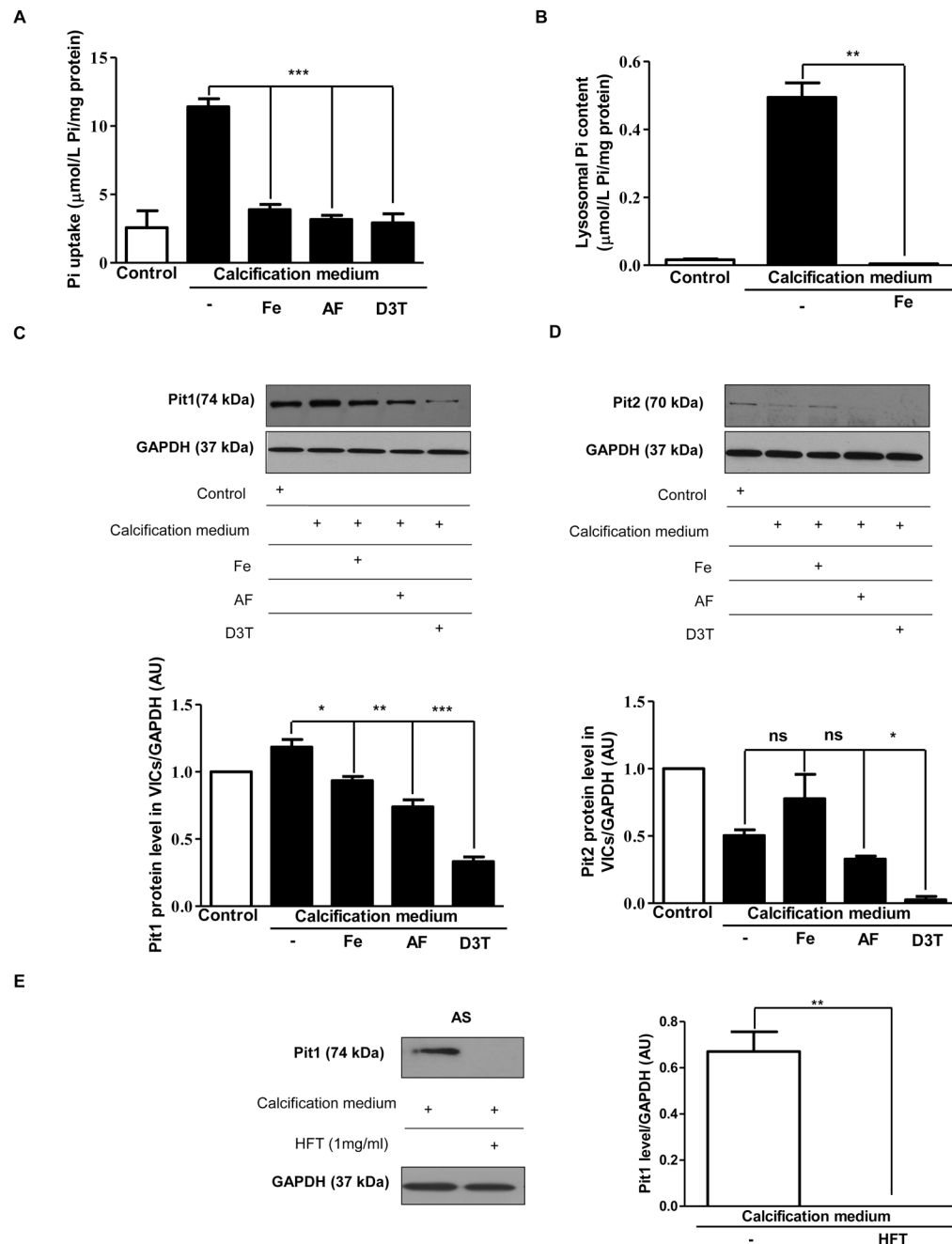


**Figure 4. Phosphate uptake by valvular interstitial cells is reduced by iron, apo-ferritin, and D3T**

A) Cells were cultured in a normal or calcific environment exposed to iron, or apo-ferritin, or D3T and phosphate content was determined using QuantiChrom quantitative colorimetric assay. B) VIC was cultured in growth medium or calcification medium in the presence or absence of iron (Ammonium iron (III) citrate). After isolation of lysosomes, phosphate level was measured. VIC was cultured with 50  $\mu\text{mol/L}$  iron (Ammonium iron (III) citrate), 2 mg/mL apo-ferritin, 75  $\mu\text{mol/L}$  D3T and C) Pit1 and D) Pit2 Western blotting was performed in the same experiments. E) VIC derived AS valves were cultured in calcific condition alone or supplemented with H-ferritin. Pit1 Western blots were carried out and

normalized to the protein content of the samples. Results were analyzed by One Way ANOVA, Bonferroni's Multiple Comparison Test and are shown as mean values  $\pm$  SEM of at least three independent experiments. \*P < 0.05; \*\*P < 0.001; \*\*\*P < 0.0001.

Author Manuscript

Author Manuscript

Author Manuscript

Author Manuscript

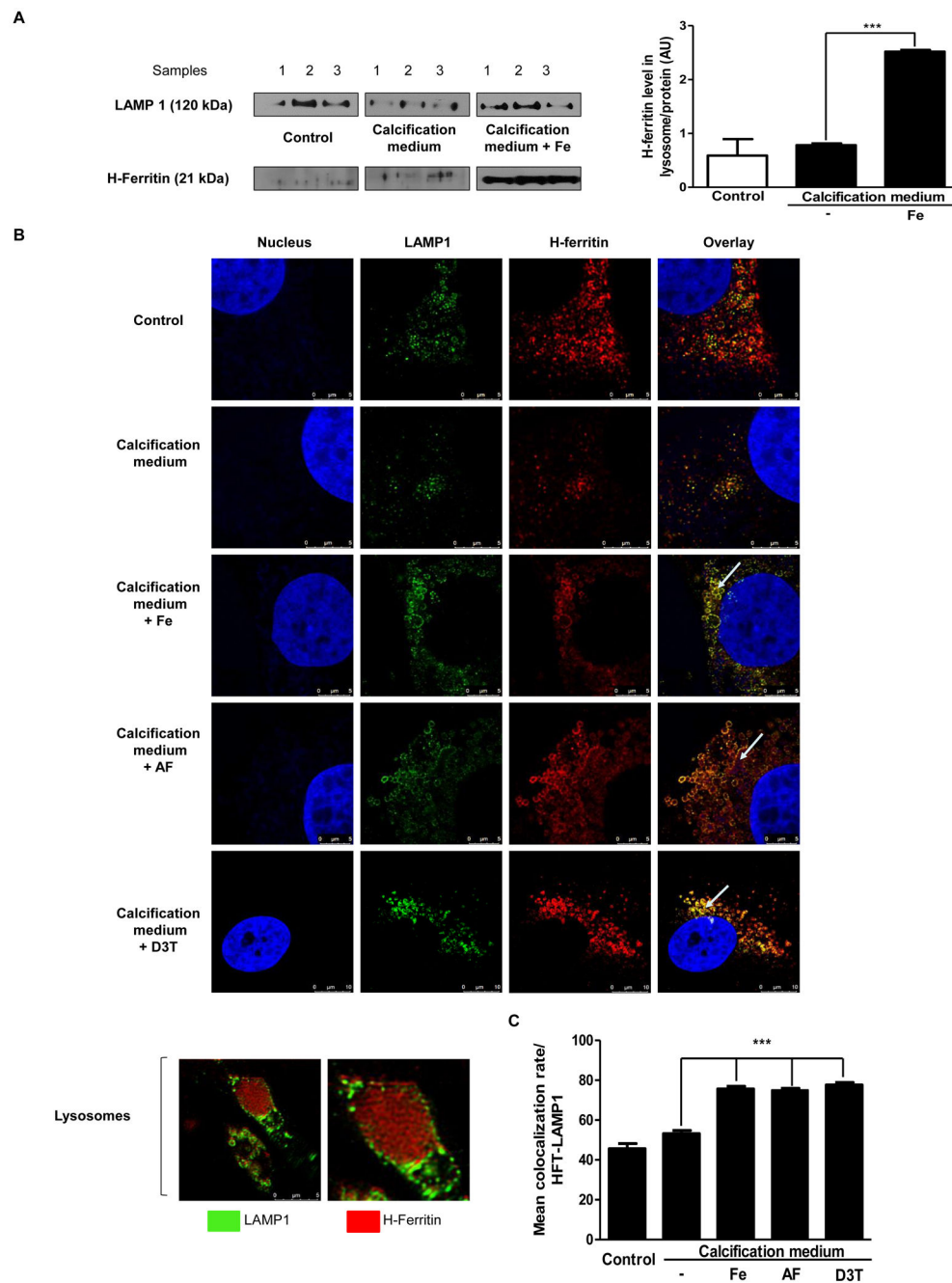


**Figure 5. Lysosomal localization of H-ferritin in cells exposed to iron, apo-ferritin or D3T**

A) VIC was cultured in growth medium or calcification medium in the presence or absence of iron (Ammonium iron (III) citrate). Western blot analysis for H-ferritin and LAMP1 derived from the isolated lysosome. B) VIC was cultured in growth medium or calcification medium in the presence or absence of iron (Ammonium iron (III) citrate), apo-ferritin or D3T. Double immunofluorescence staining of VIC for LAMP1 and H-ferritin are shown. Images were obtained employing immunofluorescence-confocal microscope and STED nanoscopy. Representative staining is shown from at least three independent experiments.

Results were analyzed by One Way ANOVA, Bonferroni's Multiple Comparison Test and are shown as mean values  $\pm$  SEM of at least three independent experiments. \*\*\*P < 0.0001.

Author Manuscript

Author Manuscript

Author Manuscript

Author Manuscript

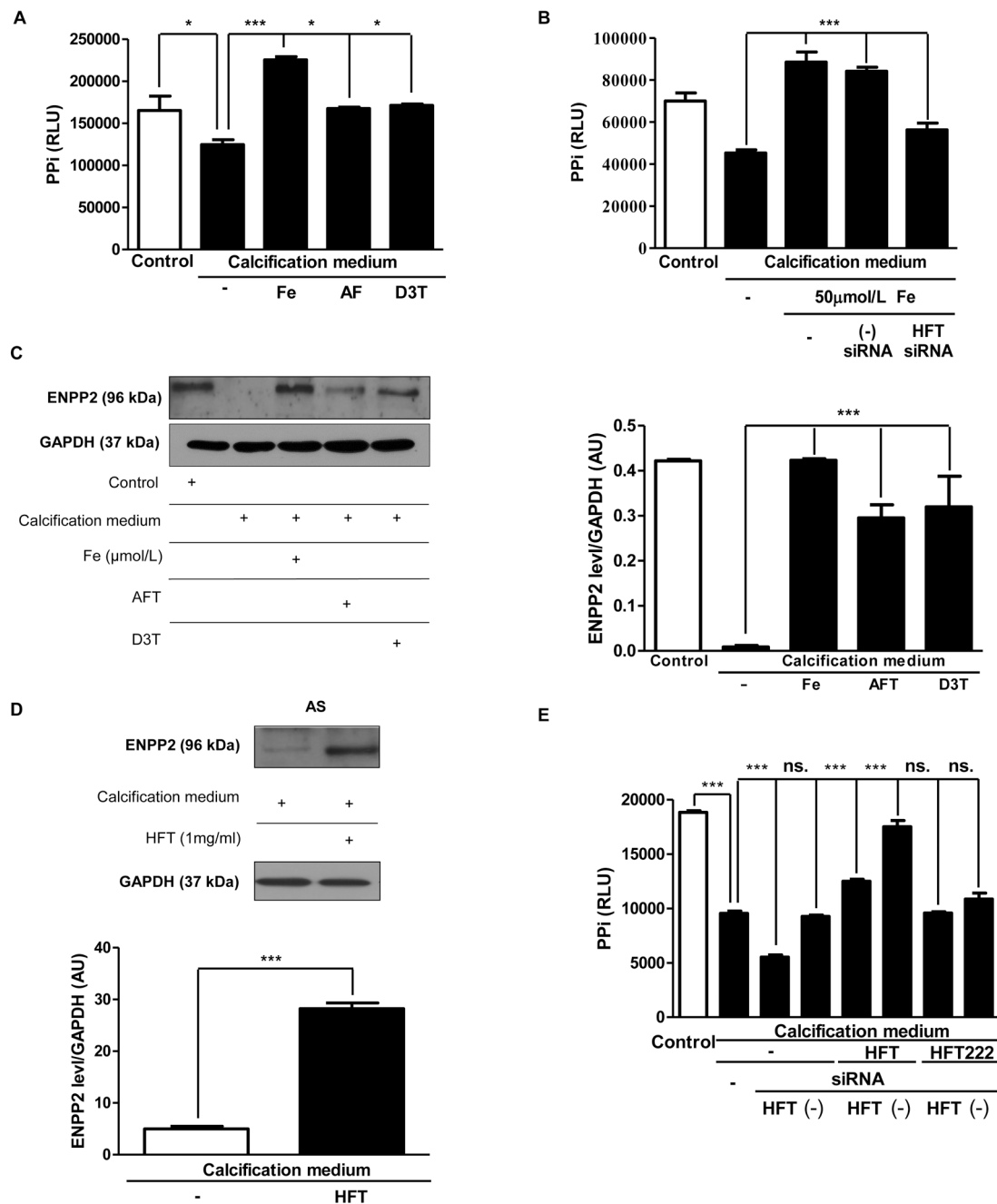


**Figure 6. Pyrophosphate generation and ENPP expression are enhanced in VIC by iron, apo-ferritin and D3T.**

A) VIC was cultured in growth or calcification medium supplemented with 50  $\mu\text{mol/L}$  iron (Ammonium iron (III) citrate), 2 mg/mL apo-ferritin or 75  $\mu\text{mol/L}$  D3T for five days and pyrophosphate level was measured. B) VIC was transfected with siRNA specific to H-ferritin or negative control siRNA prior to iron exposure and pyrophosphate level was measured. C) ENPP2 expression in VIC was assessed by Western blot analysis. D) ENPP2 Western blot were shown. AS tissues derived VIC cells were cultured in calcific condition alone or treated with H-ferritin. Samples were normalized to the protein content of the cells.

E) PPI level changes after H-Ferritin silencing were shown. VIC cells were transfected with siRNA against H-Ferritin. Samples were treated in the next day with 1 mg/mL of H-Ferritin and 1 mg/mL H-Ferritin 222 (mutant ferritin without ferroxidase activity) for 3 days. Data were analyzed by One Way ANOVA, Bonferroni's Multiple Comparison Test and are shown as mean values  $\pm$  SEM of three separate experiments performed in duplicate. Not significant (ns), \*P < 0.05; \*\*\*P < 0.0001.

Author Manuscript

Author Manuscript

Author Manuscript

Author Manuscript

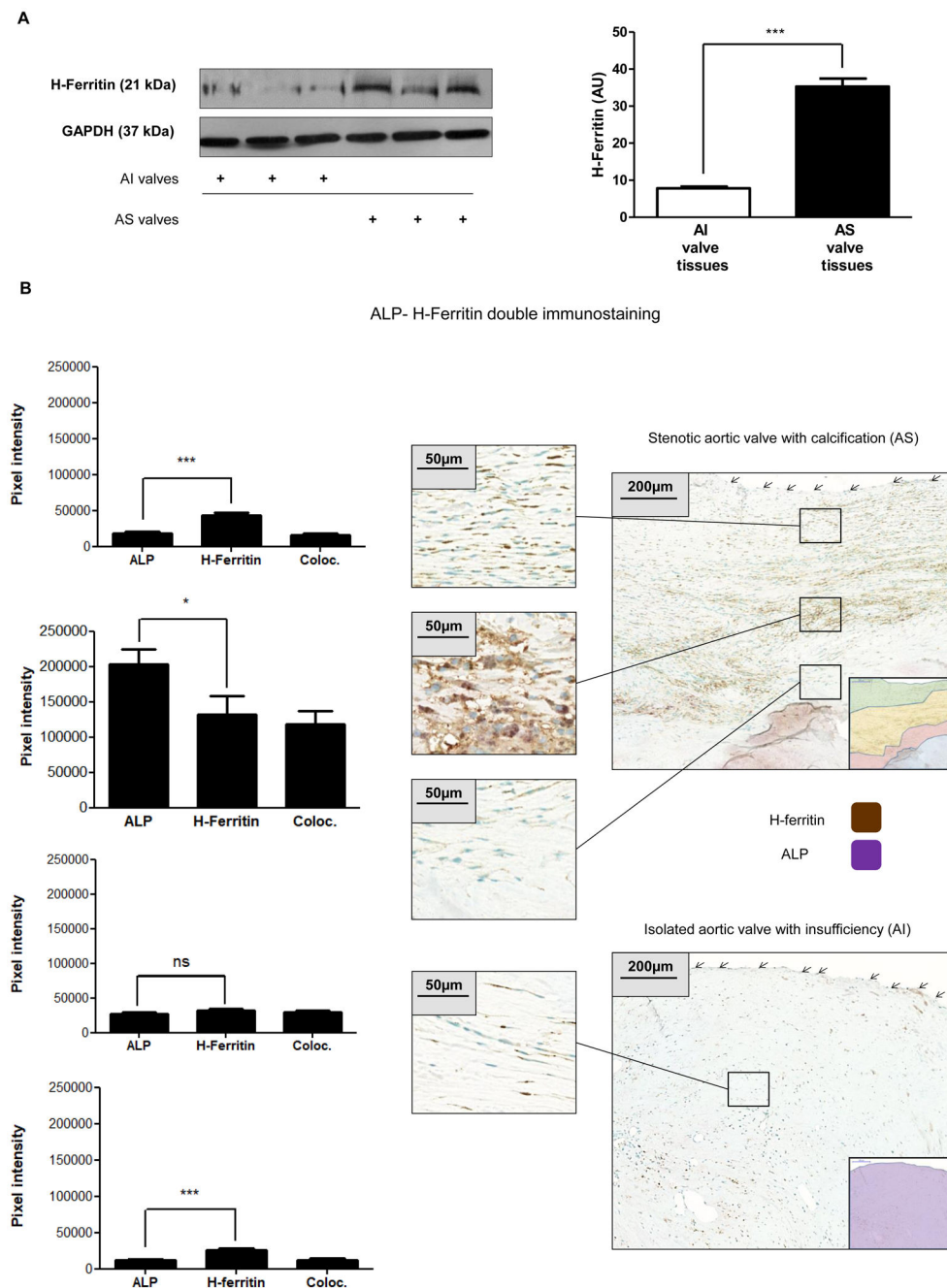


**Figure 7. H-ferritin expression in AI and AS heart valves**

A) H-ferritin expression in AI and AS heart valve tissue was assessed by Western blot analysis. B) The AI and AS valve sections were stained for ALP and H-ferritin. ALP, H-ferritin and colocalization rate of ALP and H-ferritin are shown as pixel intensity from AS and AI samples (left panels). Arrows show endothelial layer. Scale bars show 200  $\mu\text{m}$  at 12.5x magnification and 50 $\mu\text{m}$  at 50x magnification. Results were analyzed by Unpaired t-test and are shown as mean values  $\pm$  SEM of at least three independent experiments.



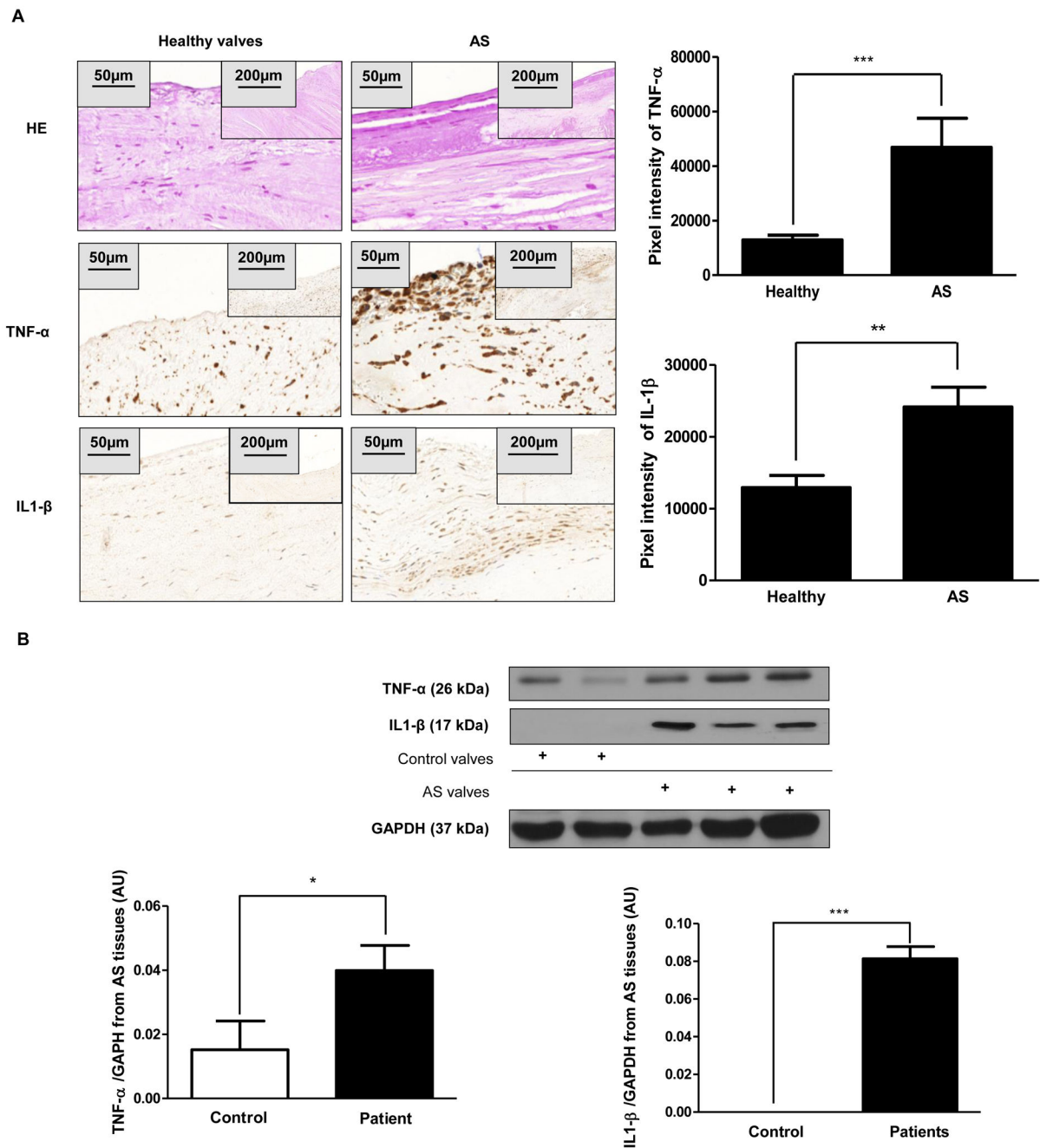


**Figure 9. Increased expression of inflammatory markers in AS valves**

A) Hematoxylin and eosin (upper panels); TNF- $\alpha$ ; and IL-1- $\beta$  IHC staining were performed on healthy heart valves derived from the Department of Forensic Institute, University of Debrecen (left column; N=3) and on AS valves with calcification (right column, N=9). Scale bars (200  $\mu$ m at 12.5x magnification and 50  $\mu$ m at 50x magnification) and pixel intensity of IHC staining were shown. Representative staining was shown from at least three independent experiments. B) Western blots (TNF- $\alpha$  and IL-1- $\beta$ ) from AS tissues were shown. Protein expressions were normalized to GAPDH. Results were analyzed by One

Way ANOVA, Bonferroni's Multiple Comparison Test (Figure 8B) and were shown as mean values  $\pm$  SEM of at least three independent experiments. \*\*P < 0.001; \*\*\*P < 0.0001.

Author Manuscript

Author Manuscript

Author Manuscript

Author Manuscript

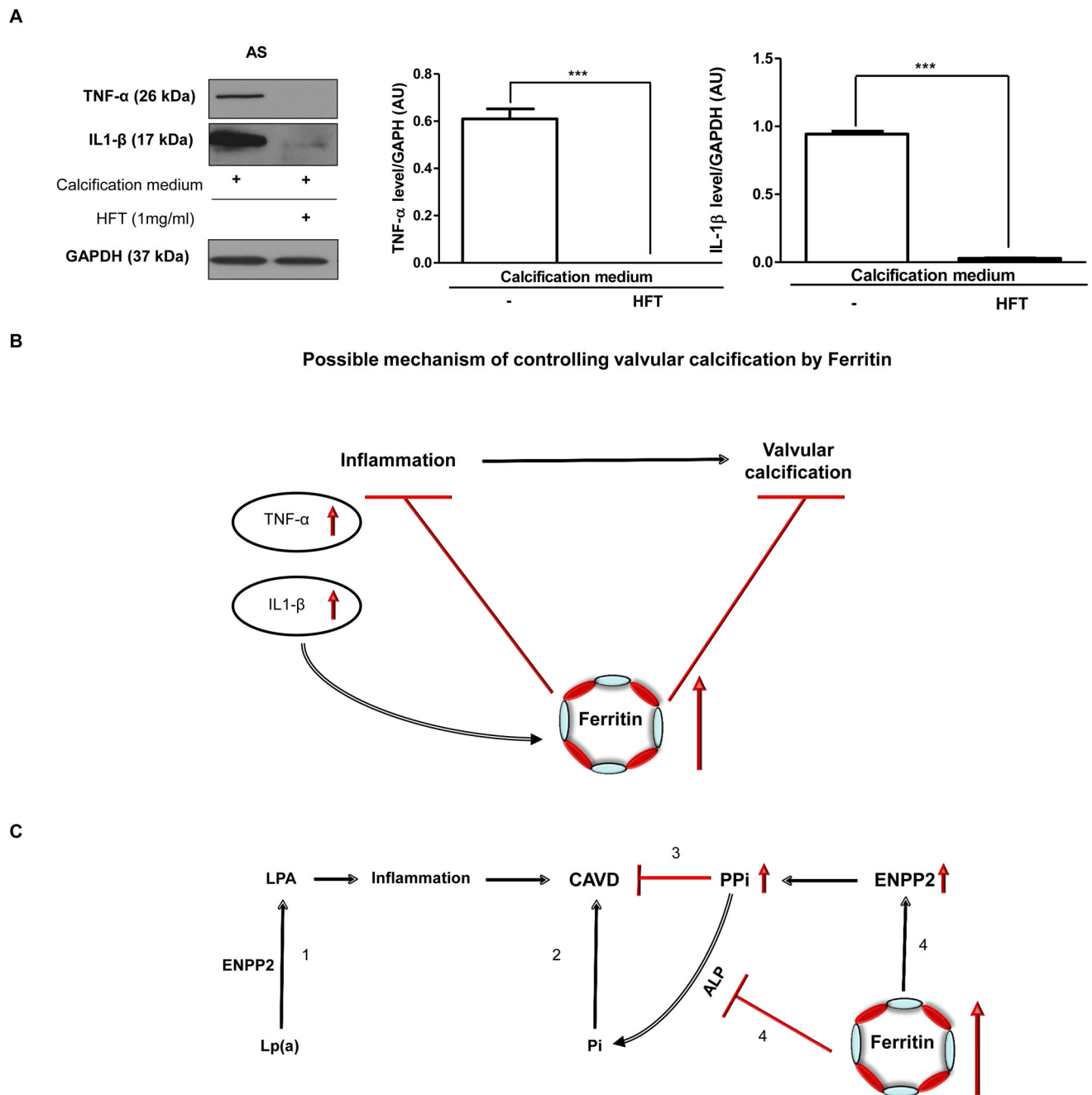


**Figure 10. H-ferritin inhibits the expression of TNF- $\alpha$  and IL1- $\beta$  in VIC derived from AS**  
 VIC was cultured in calcification medium or supplemented with 1mg/mL H-ferritin. A) Western blot was performed and the following antibodies were used: anti-human TNF- $\alpha$ ; anti-human IL1- $\beta$ . B) TNF- $\alpha$  and IL1- $\beta$  protein level in AS valve tissue. (N=3). B) Role of H-ferritin in the inflammatory process and valvular calcification. C) (1) Lp(a) is a risk factor of calcific aortic valve disease (CAVD) via inducing inflammation. (2) Pi is risk factor of calcific aortic valve disease. (3) PPI antagonizes valvular mineralization. (4) H-ferritin inhibits valvular mineralization via elevating PPI and decreasing Pi by the induction of ENPP2 and the inhibition of ALP activity. Data were analyzed by One Way ANOVA,

Bonferroni's Multiple Comparison Test and samples were derived from four separate experiments performed in triplicates and shown as mean  $\pm$  SEM \*\*\*P < 0.0001.

Author Manuscript

Author Manuscript

Author Manuscript

Author Manuscript